DNA packaging via hierarchical chromatin structures revealed by live-cell 3D imaging

Yang Zheng[1,2,9], Sen Ye[1,9], Shumin Li[3,9], Cuifang Liu[4,5], Shihang Luo[5,7], Yanqin Chen[2], Yunsheng Li[2], Lingyi Huang[2], Shan Deng[1], Ping Chen[4,8], Yongdeng Zhang[2], Wei Ji[5,7], Ruibang Luo[3], Guohong Li[4,5,6]* & Dan Yang[1,2]*

[1]Morningside Laboratory for Chemical Biology and Department of Chemistry, The University of Hong Kong, Hong Kong, China.

[2]School of Life Sciences, Westlake University, Hangzhou, Zhejiang, China.

[3]Department of Computer Science, The University of Hong Kong, Hong Kong, China.

[4]National Laboratory of Biomacromolecules, CAS Center for Excellence in Biomacromolecules, Institute of Biophysics, Chinese Academy of Sciences, Beijing, China.

[5]College of Life Science, University of Chinese Academy of Sciences, Beijing, China.

[6]Bioland Laboratory (Guangzhou Regenerative Medicine and Health Guangdong Laboratory), Guangzhou, Guangdong, China.

[7]Institute of Biophysics, Chinese Academy of Sciences, Beijing, China

[8]Department of Immunology, School of Basic Medical Sciences, Advanced Innovation Center for Human Brain Protection, Capital Medical University, Beijing, China.

[9]These authors contributed equally: Yang Zheng, Sen Ye, Shumin Li.

*Correspondence: Guohong Li (liguohong@ibp.ac.cn) or Dan Yang (yangdan@westlake.edu.cn)

ABSTRACT

How the 2-m-long genomic DNA is packaged into chromatin in the 10-μm eukaryotic nucleus is a fundamental question in cell biology. DNA accessibility depends on chromatin structure and dynamics, which basically control all DNA-related processes, such as transcription, DNA replication and repair.

The hierarchical model of chromatin organization has been controversial in recent years because live-cell evidence for the existence of chromatin fibers, particularly those 30 nm in diameter, has remained elusive. Herein, we report a DNA-binding, fluorogenic and self-blinking small-molecule probe for the first live-cell 3D superresolution imaging of chromatin fibers with structural plasticity and fast dynamics. Our live-cell imaging results suggest a model of DNA packaging in interphase with the hierarchical organization of nucleosomal arrays and chromatin fibers.

INTRODUCTION

How the 2-m-long genomic DNA is packaged into the 10-μm eukaryotic nucleus is a fundamental question. The classic model proposes that DNA is hierarchically packaged by histones into chromatin, which is organized into "beads-on-a-string" nucleosomal arrays, compact 30-nm chromatin fibers and even larger fibers beyond 30 nm in diameter[1-3]. DNA accessibility, controlled by dynamic chromatin organization, is critical for all DNA-dependent processes, including gene transcription and DNA replication and repair. However, the hierarchical model of chromatin organization has been controversial in recent years[5-14] due to the paucity of live-cell evidence for the existence of compact chromatin fibers, particularly those with a diameter of 30 nm. On the one hand, structures revealed *in vitro* do not necessarily represent native chromatin structures in living cells. Moreover, there are inevitable artifacts associated with *in vitro* approaches. For instance, the ChromEMT approach relies on a tedious and harsh sample preparation process of cell fixation, DRAQ5 staining, photooxidation and subsequent oxidative polymerization of diaminobenzidine (DAB), OsO_4 staining, EtOH dehydration and resin embedding[12]. What was stained by OsO_4 was not chromatin but the polymer of oxidized DAB. The native chromatin ultrastructure could have been damaged by photooxidation before electron microscopy (EM) analysis. On the other hand, live-cell superresolution microscopy approaches failed to reveal 3D chromatin structures with sufficient spatiotemporal resolution and labeling density[10,11,13,15-18]. Taken together, these prior studies furnished only a limited understanding of chromatin structure and dynamics in living cells.

To address this puzzle, it is essential to develop a 3D superresolution imaging method for native chromatin structures in living cells with high spatiotemporal resolution and labeling density at modest laser intensity. For this purpose, a highly selective DNA-binding, self-blinking and fluorogenic probe, **6-HoeHESiR**, has been developed with its "ON" state population properly fine-tuned to quickly achieve high labeling density and minimize motion blur. This new probe has been validated by single-molecule localization microscopy (SMLM) with *in vitro* reconstituted nucleosomal arrays and 30-nm chromatin fibers, and our 3D imaging results are consistent with EM images. The 3D visualization of both nucleosomal arrays and chromatin fibers in living cells has been achieved with high spatiotemporal resolution and labeling density, even at reduced laser intensity for lower phototoxicity. We observed structural plasticity of chromatin fibers with 35- to 40-nm mean diameters. Fast chromatin fiber dynamics were captured with less than 2-second temporal resolution, and the mean resting/dwelling lifetime of chromatin fibers in living HeLa cells was estimated to be 0.6 seconds. With this novel probe, we were able to observe the decompaction of chromatin fibers induced by small-molecule inhibitors of histone deacetylases (HDACs), providing the first live-cell evidence for the tight connection between the histone acetylation state and 3D chromatin organization with unprecedented resolution.

RESULTS

The development of a DNA-binding, fluorogenic and self-blinking probe

Superresolution fluorescence microscopy is a powerful tool for interrogating important biological questions. By bypassing the diffraction limit of light, superresolution microscopy has been developed to visualize previously unresolvable fine subcellular structures with nanometer-scale precision[19-24]. The commercial organic dyes (e.g., Alexa 647) widely used for SMLM still suffer from poor cell permeability and photoswitching buffers that are highly reducing and incompatible with live cells[24]. Such limitations have impeded the study of important biological questions by live-cell SMLM. To overcome this bottleneck, we endeavor to develop new organic fluorophores with the following criteria: 1) self-blinking with an absorption maximum in the deep red and near infrared regions to minimize

autofluorescence and phototoxicity to living cells[25] and 2) a fine-tuned percentage of the fluorescent "ON" state for optimal localization number per frame to achieve sufficient labeling density in a short acquisition time while preventing signal overlap[24]. Urano group pioneered the self-blinking silicon-rhodamine fluorophore **HMSiR** for live-cell SMLM[26]. However, currently there has been no effort to fine-tune the self-blinking "ON" state population for optimal imaging quality and performance. Therefore, we rationally designed a new self-blinking Si-rhodamine fluorophore, **6-HESiR**, according to our design strategy (Fig. 1a-b). By replacing the hydroxymethyl group on the upper ring of **HMSiR** with a hydroxyethyl group[26-28], the cyclization/ring opening self-blinking equilibrium is shifted toward the open, fluorescent "ON" state. This new fluorophore **6-HESiR** was successfully prepared with an efficient synthetic route (Supplementary Information, chemical synthesis section), and it could potentially increase the localization number per frame significantly for the fast acquisition of sufficient localizations to resolve dynamic fine structures. The "ON" state population of **6-HESiR** was found to be 20% at physiological pH in aqueous buffer with **SiR650** as the benchmark of the 100% "ON" state (Fig. 1b-d), and the pK_{cycl} value of **6-HESiR** was determined to be 6.6 (based on its pH titration curve, Fig. 1e; Supplementary Fig. 1a), higher than that of **HMSiR** (pK_{cycl} = 5.8, Fig. 1a).

The successful implementation of live-cell SMLM hinges not only on the self-blinking fluorophore but also on a fully biocompatible labeling strategy that is noninvasive, highly selective, and artifact-free with high labeling density. In this regard, we chose the Hoechst tagging strategy, as it has found some success in developing fluorogenic probes for live-cell chromatin imaging[13,16,17,29-31] with low cytotoxicity. The Hoechst moiety could perform highly selective noncovalent binding to the DNA minor groove with negligible linkage error between the target DNA molecule and our novel self-blinking dye **6-HESiR**. Therefore, we designed and synthesized **6-HoeHESiR** by connecting **6-HESiR** and the Hoechst fragment with a carbamate linker (Fig. 2a). The *in vitro* binding of **6-HoeHESiR** to a benchmark hairpin DNA (hpDNA) molecule (Fig. 2b) with an AATT Hoechst binding site[32] was studied by fluorescence titration. In the absence of hpDNA, the fluorescence of **6-HoeHESiR** was

nearly quenched (Fig. 2c). A dose-dependent fluorescence turn-on was observed upon the addition of increasing equivalents of hpDNA to **6-HoeHESiR** (Fig. 2c). A 43-fold fluorescence increase with 14 μM of hpDNA confirmed the sensitivity and fluorogenicity of **6-HoeHESiR**. Based on the titration curve, the dissociation constant (K_D) of the complex formed by **6-HoeHESiR** and hpDNA was estimated to be 3.8 μM. Attachment of **6-HESiR** to the Hoechst dye caused a slight redshift of both the absorbance and fluorescence maxima of **6-HoeHESiR**. Upon the addition of hpDNA (14 μM), the absorbance of **6-HoeHESiR** was increased to a level close to that of the free fluorophore **6-HESiR** (Supplementary Fig. 2a), and the fluorescence of **6-HoeHESiR** was recovered to 21% of that of **6-HESiR** (Fig. 2d).

SMLM with *in vitro* lambda DNA and reconstituted chromatin structures

To evaluate our new probe **6-HoeHESiR**, we first attempted an SMLM experiment of spin-coated lambda DNA[33] with $(A/T)_4$ binding sites for the Hoechst moiety[32]. A full width at half maximum (FWHM) of 26 nm was successfully obtained (Supplementary Fig. 3), within the range of 20–30 nm as reported in literature. Then, we focused on *in vitro* reconstituted nucleosomal arrays and 30-nm chromatin fibers as benchmarks well characterized by EM[34] (Fig. 3d and 3g; Supplementary Fig. 4a and 4e). Apart from the AATT binding site, three additional Hoechst binding sites[32] in the DNA template for *in vitro* reconstituted chromatin samples were also identified by fluorescence titration (Fig. 3a and 3b; Supplementary Fig. 2b-d). Based on the dissociation constants, the half-life of the complex formed by **6-HoeHESiR** and a nucleosome was estimated to be 10-20 ms[32]. Thus, fast binding/dissociation cycles between **6-HoeHESiR** and nucleosomes could allow fast self-blinking with a pool of **6-HoeHESiR** molecules in the unbound state (Fig. 2e). Since the hydrophobic environment in the nucleus favors the closed "OFF" state[27] (Fig. 1b) and the open form of **6-HoeHESiR** in the unbound state is nearly quenched in fluorescence (Fig. 2c), the "ON" state population of **6-HoeHESiR** in chromatin imaging is expected to be lower than the 20% "ON" fraction of **6-HESiR** measured in aqueous buffer. Gratifyingly, **6-HoeHESiR** exhibited excellent self-blinking in SMLM experiments on reconstituted chromatin

samples at a modest laser intensity[25] of 950 W/cm^2 (Supplementary Video 1). The reconstituted nucleosomal arrays displayed the pattern of discrete fluorescence signals (Fig. 3c and 3e; Supplementary Fig. 4b), which resembles the EM images (Fig. 3d; Supplementary Fig. 4a). Analysis of localizations on individual nucleosomes indicated that the ratio of axial to lateral resolution is 2.3 (Supplementary Fig. 4c and 4d). To extract 3D structural features of reconstituted 30-nm chromatin fibers visualized in 3D SMLM experiments (Fig. 3f and 3h; Supplementary Fig. 4f), we developed an image analysis framework/program (Supplementary Information, image analysis section). Statistical results showed that the reconstituted chromatin fibers had a mean diameter of 33 nm, length of 114 nm, mean localization precision of 7.8 nm and labeling density of 32,944 molecules/μm^3 (Supplementary Fig. 4g; Supplementary Video 2 and 3). Although the reconstituted 30-nm fibers without biotin labels were visualized by EM in a dry and flattened state (Supplementary Information, EM analysis section), unlike our 3D SMLM approach, the 3D structural features obtained with **6-HoeHESiR** were consistent with those revealed by EM (Fig. 3h and 3i). Some elongated fibers were observed, probably due to slight loosening in the aqueous buffer (without glutaldehyde as a crosslinker) compared with the dry state in EM analysis.

Hierarchical chromatin structures in living cells

Building upon the solid validation of **6-HoeHESiR** with benchmark *in vitro* reconstituted nucleosomal arrays and 30-nm chromatin fibers, we then attempted to image native chromatin structures in living cells. First, we optimized the incubation conditions of **6-HoeHESiR** with living HeLa cells by light-sheet microscopy (Fig. 4a and 4b; Supplementary Fig. 5a and 5b). To our delight, **6-HoeHESiR** exhibited good cell permeability and high selectivity to provide 3D visualization of chromatin structures in whole nuclei. Without the Hoechst fragment, **6-HESiR** did not stain any nuclear component (Supplementary Fig. 5c). Cytotoxicity assay showed that **6-HoeHESiR** caused negligible toxicity with a short incubation time (Supplementary Fig. 5d). Subsequent 3D SMLM experiments showed that **6-HoeHESiR** maintained its excellent self-blinking capacity in living HeLa cells (Supplementary Video

4), and chromatin structures were clearly revealed (Fig. 4c; Supplementary Fig. 6a). Based on the structural resemblance to *in vitro* reconstituted benchmark chromatin samples, we identified two categories of chromatin structures in living HeLa cells. The first category consists of nucleosomal arrays (Fig. 4d), which displayed the same pattern of discrete fluorescence signals (Fig. 3d and 3e). The second category consists of chromatin fibers (Fig. 4e; Supplementary Fig. 6b). With the aid of the same image analysis program, these fibers were identified with a mean localization precision of 7.5 nm, short and long fiber diameters of 33 and 44 nm, and a labeling density of 32,996 molecules/μm^3 (Fig. 4f; Supplementary Fig. 6c; Supplementary Video 5 and 6). The statistical distribution of 3D sizes and long-to-short fiber diameter ratios and the heterogeneity of structural characteristics could reflect the structural plasticity/polymorphism of chromatin fibers involved in highly sophisticated biological functions[1-3]. Our 2D imaging results are consistent with recent reports[10,11,13] that nucleosome clutches or chromatin domains were observed with no clear evidence of horizontally or randomly oriented chromatin fibers. However, our 3D analysis, performed both manually and by the computer program, identified chromatin fibers oriented axially or slightly tilted from the vertical axis. We propose that such an ordered chromatin fiber orientation might not only be consistent with highly regulated replication and transcription processes but facilitate these processes. The overlay of widefield images showed that the chromatin fibers reside in both the peripheral and the interior regions of the nuclei (Fig. 4g; Supplementary Fig. 6d). Remarkably, chromatin structures in the nucleus are quite dynamic (Supplementary Video 7). We were able to capture transient chromatin fibers with a temporal resolution of less than 2 seconds (Fig. 4h; Supplementary Video 8). The mean resting/residing lifetime of chromatin fibers was estimated to be 0.6 seconds (Supplementary Fig. 6e), implying fast-turnover transitions that are consistent with fast transcription activities. This dwelling lifetime is comparable to the time scale of folding and unfolding dynamics of *in vitro*-reconstituted 30-nm chromatin fibers revealed by single-molecule force spectroscopy[34]. The structural plasticity and fast dynamics of chromatin fibers might be closely associated with complex regulatory factors, including histone variants

and modifications, chromatin remodelers, and histone chaperons[1-3], for the regulation of DNA accessibility and activities. When the laser intensity was reduced to a modest level of 950 W/cm^2 from 3.2 kW/cm^2 to alleviate phototoxicity, nucleosomal arrays were visualized again, and we could still identify chromatin fibers at sufficient resolution with a mean localization precision of 8.8 nm, short and long fiber diameters of 33 and 42 nm, and a labeling density of 29,436 molecules/μm^3 (Supplementary Fig. 7a-f). Fast chromatin dynamics were also revealed, and the mean resting lifetime of chromatin fibers was estimated to be 0.6 seconds (Supplementary Video 9; Supplementary Fig. 7g), similar to the result obtained under 3.2 kW/cm^2 laser intensity.

A previous cryo-electron tomography (cryo-ET) study identified short chromatin fibers with 30 nm in diameter in isolated nuclei from chicken erythrocytes[7]. Therefore, we also attempted 3D SMLM experiments on living chicken erythrocytes with **6-HoeHESiR**. By applying a modest laser intensity of 950 W/cm^2, 3D chromatin structures in chicken erythrocyte nuclei were successfully visualized (Fig. 5a-c; Supplementary Fig. 8a; Supplementary Video 10). The same two categories of chromatin structures were observed, and chromatin fibers were identified with a mean localization precision of 8 nm, short and long fiber diameters of 29 and 37 nm, and a higher labeling density of 56,359 molecules/μm^3 (Fig. 5d-g; Supplementary Fig. 8b-d; Supplementary Video 11 and 12). The fast dynamics of chromatin structures in chicken erythrocyte nuclei were also observed (Supplementary Video 13), with the mean resting lifetime of chromatin fibers estimated to be 1 second (Supplementary Fig. 8e).

The connection between 3D chromatin organization and histone acetylation

A previous study showed that histone acetylation is a critical epigenetic marker for chromatin fiber relaxation and optimal transcription, while deacetylation is required for chromatin fiber condensation and transcriptional repression[35]. Histone deacetylases (HDACs), key enzymes that modulate acetylation, can be important drug targets to counteract abnormal protein acetylation status, induce chromatin decompaction, and reactivate tumor suppressor genes[36,37]. To investigate the connection between

chromatin fibers and histone acetylation in living cells, we selected three HDAC inhibitors (Fig. 6a): 1) trichostatin A (TSA), a widely used HDAC pan-inhibitor; 2) entinostat, a class I HDAC 1−3 selective inhibitor; and 3) ricolinostat, a class IIb HDAC 6 selective inhibitor. Live HeLa cells were treated with these HDAC inhibitors and then imaged by 3D SMLM (Fig. 6b). The results showed that the density of chromatin fibers decreased by 52% and 63% upon TSA and entinostat treatments, respectively (Fig. 6c and 6d; Supplementary Fig. 9 and 10). However, no significant change in fiber density was observed upon ricolinostat treatment (Fig. 6c and 6d; Supplementary Fig. 11). Both the nonselective inhibition of HDACs and the selective inhibition of class I HDACs 1−3 led to decompaction of chromatin fibers[38,39]. In contrast, selective inhibition of class IIb HDAC 6 induced no significant fiber decompaction. These results are consistent with the literature reports that the functions of class I HDACs 1−3 are exclusively restricted to the nucleus, while class IIb HDAC 6 functions largely outside the nucleus by mediating the deacetylation of cytosolic proteins[40]. Taken together, our live-cell 3D imaging results provide new insights into the global change in 3D chromatin organization in response to histone hyperacetylation induced by small-molecule HDAC inhibitors.

DISCUSSION

Our findings allow us to depict genomic DNA packaging through the dynamic organization of nucleosomal arrays and chromatin fibers in living cells (Fig. 7). To the best of our knowledge, our 3D imaging results have furnished the first live-cell evidence for a hierarchical model of dynamic chromatin organization. We propose that nucleosomal arrays could be regarded as the primary chromatin structures and chromatin fibers as the secondary and higher-order structures. The structural plasticity and fast dynamics of chromatin fibers are consistent with the complex regulatory environment in the nucleus, such as histone modifications and variants, nonhistone architectural proteins, and linker DNA lengths for various biological functions[1-3]. The density/population of chromatin fibers was reduced by small-molecule inhibitors of HDACs that are responsible for histone deacetylation. For the first time,

this phenomenon provides a live-cell 3D view of the tight connection between the histone acetylation state and chromatin hierarchical organization with unprecedented resolution.

The linchpin of our success is the new self-blinking fluorogenic probe, **6-HoeHESiR**, developed according to our new design strategy to increase the self-blinking "ON" state population to a suitable level. This design strategy has resulted in high spatiotemporal resolution and labeling density even at a moderate laser intensity for reduced phototoxicity. In light of our initial success, we envision that our new design strategy could be implemented to develop more self-blinking fluorophores and probes to enable the study of subcellular organelles and biological events by live-cell 3D superresolution imaging.

Acknowledgments

We thank the HKU Li Ka Shing Faculty of Medicine Imaging and the Flow Cytometry Core of CPOS for support in cell imaging. This work was supported by The University of Hong Kong, Westlake University, Morningside Foundation, and Hong Kong Research Grants Council under the Area of Excellence Scheme (AoE/P-705/16 to D.Y.). This work was supported by grants for G.L. from the National Natural Science Foundation of China (31991161), the Ministry of Science and Technology of China (2017YFA0504202), the Beijing Municipal Science and Technology Commission (Z201100005320013) and the HHMI International Research Scholars Program (55008737). R. L. was supported by the ECS (grant number 27204518) of the Hong Kong SAR government and by the URC fund at the University of Hong Kong. We thank Dr. Teng Zhao and Dr. Zhe Hu for their technical support in light-sheet microscopy. We thank Dr. Zhe Hu, Dr. Teng Zhao, Dr. Shengwang Du and Dr. Wei Li for helpful discussions. We thank Dr. Nai-Kei Wong and Ms. Jasmine Chit Ying Lau for proofreading the manuscript.

Author contributions

Y.Z., G.L. and D.Y. conceived the project. G.L. and D.Y. supervised and directed the research. Y.Z. designed and synthesized **6-HESiR** and **6-HoeHESiR**. Y.Z. studied photophysical properties with

contributions from S.Y. C.L. prepared *in vitro*-reconstituted samples and performed electron microscopy analysis. S.-H.L. performed the SMLM experiment with lambda DNA and analyzed the data. Y.Z., S.Y. and S.D. performed cell culture and treatment. Y.Z. and S.Y. performed SMLM experiments with reconstituted chromatin structures and living cells. Y.C. and Y.L. performed the SMLM validation experiments. L.H. performed cytotoxicity assay. S.-M.L. developed the computer program and the web server for chromatin fiber analysis under the supervision of R.L. Y.Z. analyzed chromatin imaging data and performed statistical analysis with contributions from S.Y. and S.-M.L. Y.Z., S.Y., G.L. and D.Y. interpreted imaging results with contributions from all other authors. Y.Z., S.Y., G.L. and D.Y. wrote the manuscript with input from all other authors.

Competing interests

The authors declare no competing interests.

Data availability

All data that support the findings of this manuscript are provided in text, figures, and supplementary videos. Original data are provided upon reasonable request to the correspondence authors.

REFERENCES

1. Li, G. & Reinberg, D. Chromatin higher-order structures and gene regulation. *Curr. Opin. Genet. Dev.* **21**, 175-186 (2011).
2. Luger, K., Dechassa, M. L. & Tremethick, D. J. New insights into nucleosome and chromatin structure: an ordered state or a disordered affair? *Nat. Rev. Mol. Cell Biol.* **13**, 436-447 (2012).
3. Chen, P., Li, W. & Li, G. Structures and Functions of Chromatin Fibers. *Annual Review of Biophysics* **50**, 95-116 (2021).
4. Luger, K., Mäder, A. W., Richmond, R. K., Sargent, D. F. & Richmond, T. J. Crystal structure of the nucleosome core particle at 2.8 Å resolution. *Nature* **389**, 251-260 (1997).

5. Schalch, T., Duda, S., Sargent, D. F. & Richmond, T. J. X-ray structure of a tetranucleosome and its implications for the chromatin fibre. *Nature* **436**, 138-141 (2005).
6. Song, F. *et al.* Cryo-EM Study of the Chromatin Fiber Reveals a Double Helix Twisted by Tetranucleosomal Units. *Science* **344**, 376-380 (2014).
7. Scheffer, M. P., Eltsov, M. & Frangakis, A. S. Evidence for short-range helical order in the 30-nm chromatin fibers of erythrocyte nuclei. *Proc. Natl. Acad. Sci. U.S.A.* **108**, 16992-16997 (2011).
8. Risca, V. I., Denny, S. K., Straight, A. F. & Greenleaf, W. J. Variable chromatin structure revealed by in situ spatially correlated DNA cleavage mapping. *Nature* **541**, 237-241 (2017).
9. Hsieh, T.-H. S. *et al.* Resolving the 3D Landscape of Transcription-Linked Mammalian Chromatin Folding. *Molecular Cell* **78**, 539-553.e538 (2020).
10. Ricci, Maria A., Manzo, C., García-Parajo, M. F., Lakadamyali, M. & Cosma, Maria P. Chromatin Fibers Are Formed by Heterogeneous Groups of Nucleosomes In Vivo. *Cell* **160**, 1145-1158 (2015).
11. Nozaki, T. *et al.* Dynamic Organization of Chromatin Domains Revealed by Super-Resolution Live-Cell Imaging. *Mol. Cell* **67**, 282-293 (2017).
12. Ou, H. D. *et al.* ChromEMT: Visualizing 3D chromatin structure and compaction in interphase and mitotic cells. *Science* **357**, eaag0025 (2017).
13. Bucevičius, J., Gilat, T. & Lukinavičius, G. Far-red switching DNA probes for live cell nanoscopy. *Chem. Commun.* **56**, 14797-14800 (2020).
14. Lakadamyali, M. & Cosma, M. P. Visualizing the genome in high resolution challenges our textbook understanding. *Nat. Methods* **17**, 371-379 (2020).
15. Wombacher, R. *et al.* Live-cell super-resolution imaging with trimethoprim conjugates. *Nat. Methods* **7**, 717-719 (2010).

16. Bucevičius, J., Keller-Findeisen, J., Gilat, T., Hell, S. W. & Lukinavičius, G. Rhodamine–Hoechst positional isomers for highly efficient staining of heterochromatin. *Chem. Sci.* **10**, 1962-1970 (2019).
17. Bucevičius, J., Kostiuk, G., Gerasimaitė, R., Gilat, T. & Lukinavičius, G. Enhancing the biocompatibility of rhodamine fluorescent probes by a neighbouring group effect. *Chem. Sci.* **11**, 7313-7323 (2020).
18. Chi, W. *et al.* Descriptor ΔGC-O Enables the Quantitative Design of Spontaneously Blinking Rhodamines for Live-Cell Super-Resolution Imaging. *Angew. Chem. Int. Ed.* **59**, 20215-20223 (2020).
19. Liu, Z., Lavis, Luke D. & Betzig, E. Imaging Live-Cell Dynamics and Structure at the Single-Molecule Level. *Mol. Cell* **58**, 644-659 (2015).
20. Sauer, M. & Heilemann, M. Single-Molecule Localization Microscopy in Eukaryotes. *Chem. Rev.* **117**, 7478-7509 (2017).
21. von Diezmann, A., Shechtman, Y. & Moerner, W. E. Three-Dimensional Localization of Single Molecules for Super-Resolution Imaging and Single-Particle Tracking. *Chem. Rev.* **117**, 7244-7275 (2017).
22. Sahl, S. J., Hell, S. W. & Jakobs, S. Fluorescence nanoscopy in cell biology. *Nat. Rev. Mol. Cell Biol.* **18**, 685-701 (2017).
23. Sigal, Y. M., Zhou, R. & Zhuang, X. Visualizing and discovering cellular structures with super-resolution microscopy. *Science* **361**, 880-887 (2018).
24. Lelek, M. *et al.* Single-molecule localization microscopy. *Nat. Rev. Methods Primers* **1**, 39, (2021).
25. Wäldchen, S., Lehmann, J., Klein, T., van de Linde, S. & Sauer, M. Light-induced cell damage in live-cell super-resolution microscopy. *Sci. Rep.* **5**, 15348 (2015).

26. Uno, S.-n. *et al.* A spontaneously blinking fluorophore based on intramolecular spirocyclization for live-cell super-resolution imaging. *Nat. Chem.* **6**, 681-689 (2014).
27. Takakura, H. *et al.* Long time-lapse nanoscopy with spontaneously blinking membrane probes. *Nat. Biotechnol.* **35**, 773-780 (2017).
28. Uno, S.-n., Kamiya, M., Morozumi, A. & Urano, Y. A green-light-emitting, spontaneously blinking fluorophore based on intramolecular spirocyclization for dual-colour super-resolution imaging. *Chem. Commun.* **54**, 102-105 (2018).
29. Nakamura, A. *et al.* Hoechst tagging: a modular strategy to design synthetic fluorescent probes for live-cell nucleus imaging. *Chem. Commun.* **50**, 6149-6152 (2014).
30. Lukinavičius, G. *et al.* SiR–Hoechst is a far-red DNA stain for live-cell nanoscopy. *Nat. Commun.* **6**, 8497 (2015).
31. Zhang, X. *et al.* A targetable fluorescent probe for dSTORM super-resolution imaging of live cell nucleus DNA. *Chem. Commun.* **55**, 1951-1954 (2019).
32. Breusegem, S. Y., Clegg, R. M. & Loontiens, F. G. Base-sequence specificity of Hoechst 33258 and DAPI binding to five $(A/T)_4$ DNA sites with kinetic evidence for more than one high-affinity Hoechst 33258-AATT complex. *J. Mol. Biol.* **315**, 1049-1061 (2002).
33. Zhang, Y. *et al.* Ultrafast, accurate, and robust localization of anisotropic dipoles. *Protein & Cell* **4**, 598-606 (2013).
34. Li, W. *et al.* FACT Remodels the Tetranucleosomal Unit of Chromatin Fibers for Gene Transcription. *Mol. Cell* **64**, 120-133 (2016).
35. Li, G. *et al.* Highly Compacted Chromatin Formed In Vitro Reflects the Dynamics of Transcription Activation In Vivo. *Mol. Cell* **38**, 41-53 (2010).
36. Li, Y. & Seto, E. HDACs and HDAC Inhibitors in Cancer Development and Therapy. *Cold Spring Harb. Perspect. Med.* **6**, a026831 (2016).

343 37. Eckschlager, T., Plch, J., Stiborova, M. & Hrabeta, J. Histone Deacetylase Inhibitors as Anticancer
344 Drugs. *Int. J. Mol. Sci.* **18**, 1414 (2017).
345 38. Tóth, K. F. *et al.* Trichostatin A-induced histone acetylation causes decondensation of interphase
346 chromatin. *J. Cell Sci.* **117**, 4277-4287 (2004).
347 39. Otterstrom, J. *et al.* Super-resolution microscopy reveals how histone tail acetylation affects DNA
348 compaction within nucleosomes in vivo. *Nucleic Acids Res.* **47**, 8470-8484 (2019).
349 40. Fallah, M. S., Szarics, D., Robson, C. M. & Eubanks, J. H. Impaired Regulation of Histone
350 Methylation and Acetylation Underlies Specific Neurodevelopmental Disorders. *Front. Genet.* **11**,
351 613098 (2021).
352

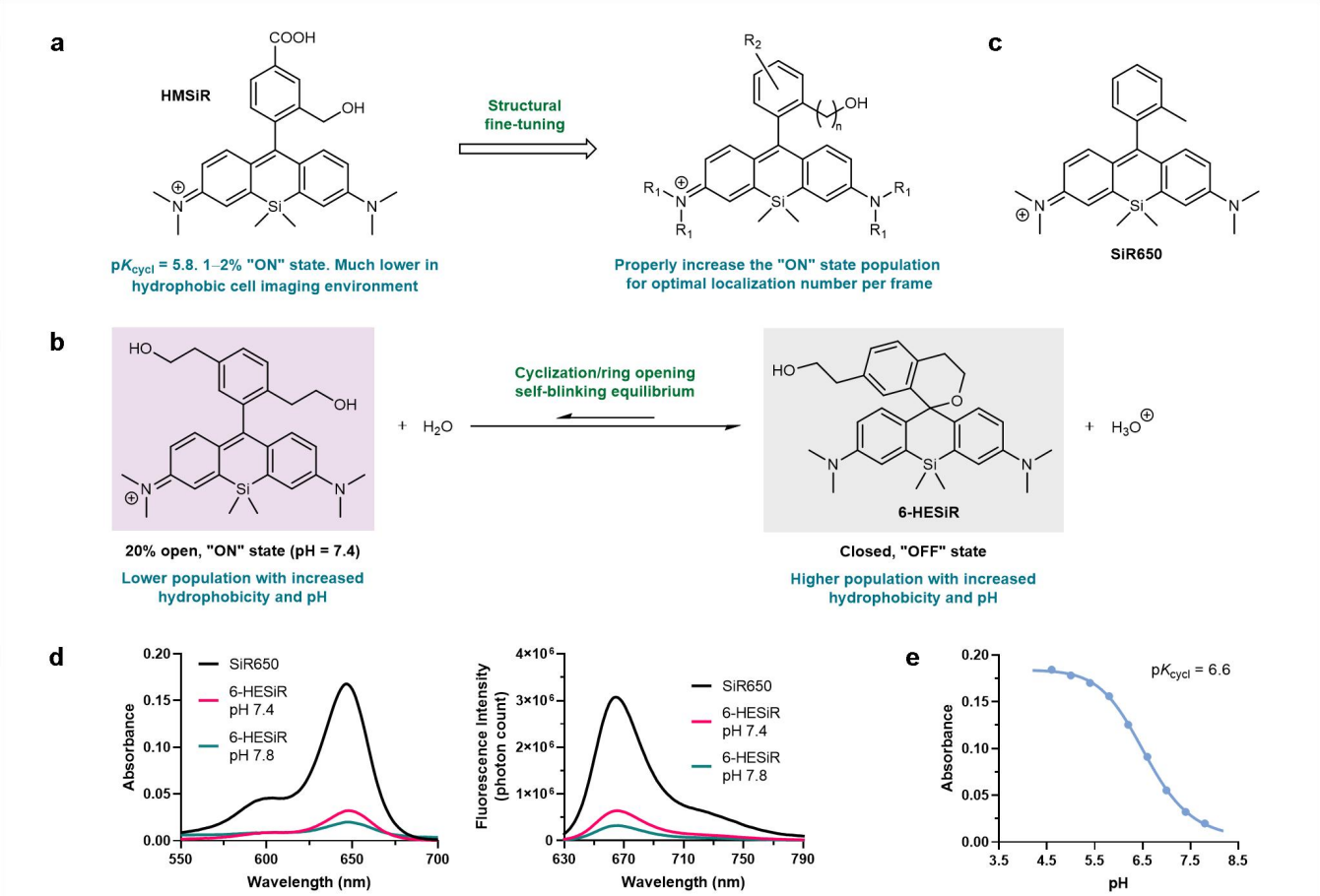

Fig. 1 Development of 6-HESiR. a, **New** design principle of developing self-blinking fluorophores. **B**, Self-blinking mechanism. **C**, Structure of **SiR650**. **D**, Absorption and fluorescence emission spectra of **6-HESiR** (2 μM) in 0.1 M potassium phosphate buffer (pH = 7.4 and 7.8) with **SiR650** (2 μM) as the "100%" benchmark. Abs_{max} at 648 nm. Fl_{max} at 665 nm. **E**, pH titration of **6-HESiR** (2 μM) in 0.1 M potassium phosphate buffer.

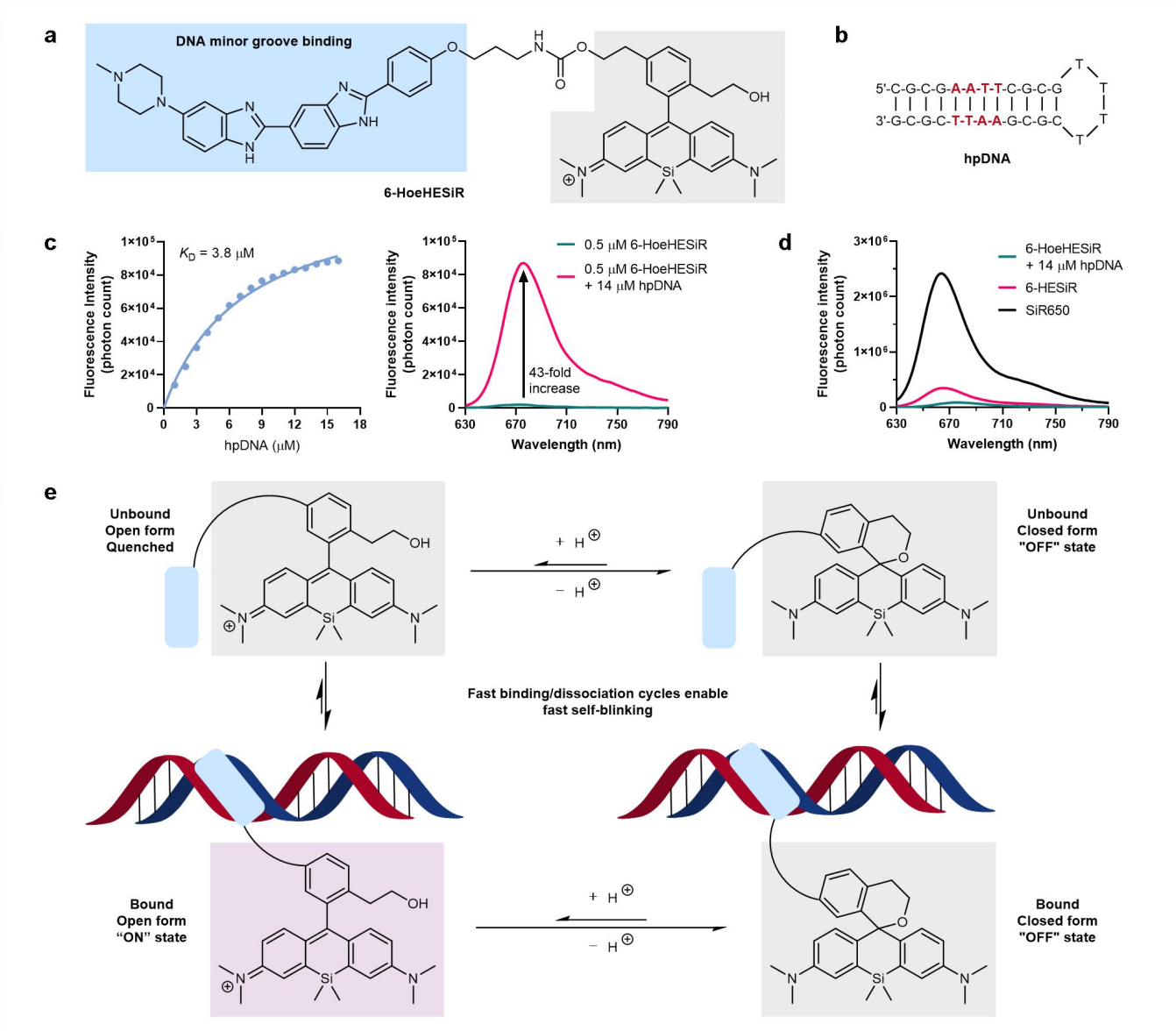

Fig. 2 Development of 6-HoeHESiR. A, **Rational** design of **6-HoeHESiR**. **b**, Structure of the hpDNA for fluorescence titration. **c**, Fluorescence titration of **6-HoeHESiR** (0.5 μM) with hpDNA (0−16 μM) in Tris-HCl saline buffer (50 mM Tris-HCl, 100 mM NaCl, pH = 7.4). Fl_{max} at 676 nm. **d**, Fluorescence of **6-HoeHESiR**, **6-HESiR** and **SiR650** (0.5 μM) in Tris-HCl saline buffer (50 mM Tris-HCl, 100 mM NaCl, pH = 7.4). **e**, Working mechanism of **6-HoeHESiR** in the presence of nucleosomes.

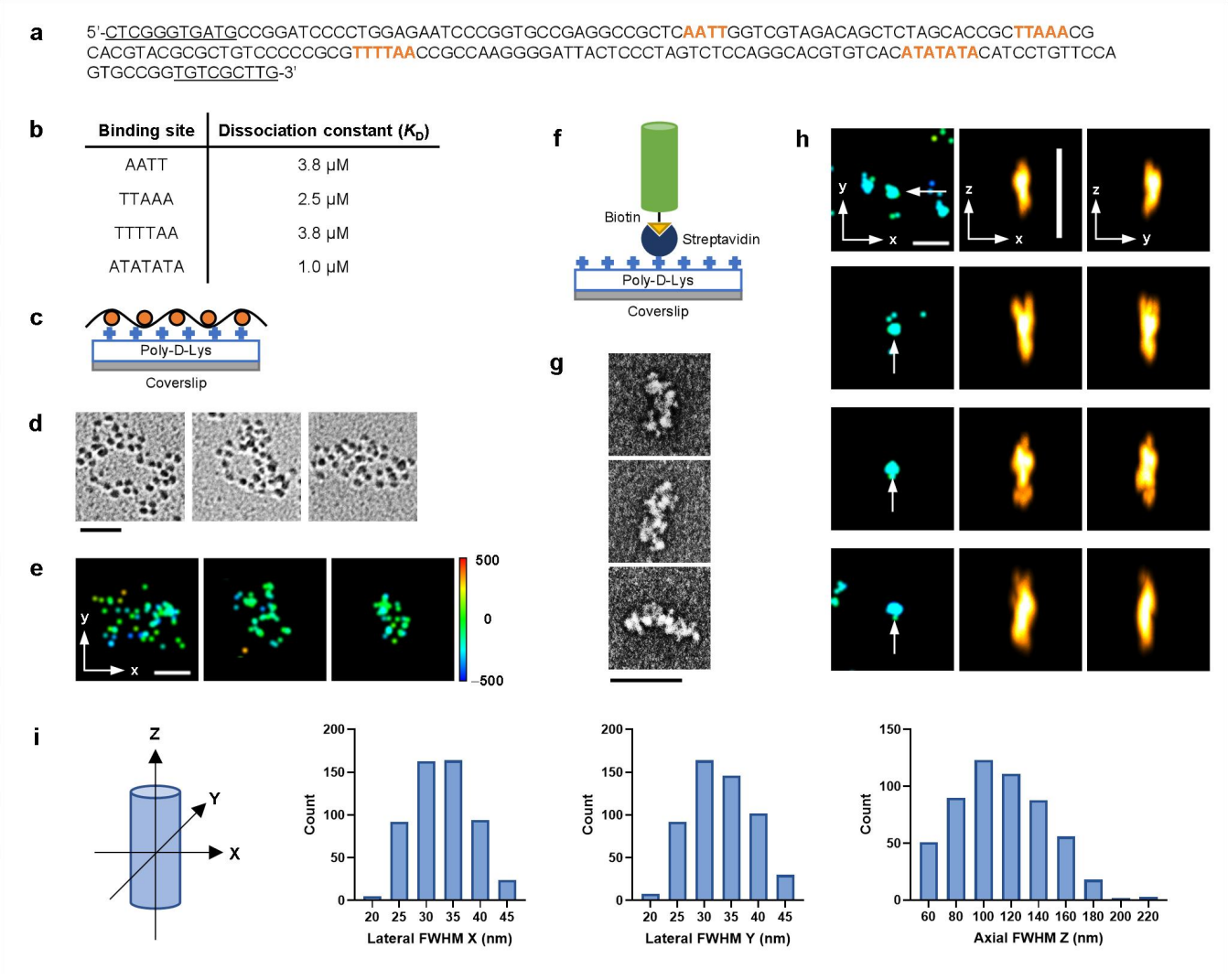

Fig. 3 *In vitro* reconstituted chromatin structures. a, Sequence of the 187-bp DNA template for reconstituted chromatin samples. The linker DNA sequence is underlined. **b**, Summary table of the dissociation constants of four binding sites in the DNA template. **c**, Immobilization approach for 40×187-bp nucleosomal arrays. **d**, EM images of 40×187-bp nucleosomal arrays (by metal shadowing). **e**, Images of 40×187-bp nucleosomal arrays by 3D SMLM. **f**, Immobilization approach for 40×187-bp 30-nm chromatin fibers. **g**, EM images of 40×187-bp 30-nm fibers (negative staining). **h**, Images of 40×187-bp 30-nm fibers by 3D SMLM. FWHM (x, y, z) in nm (from top to bottom.): 27, 29, 81; 27, 29, 96; 30, 30, 101; 34, 25, 107. Localization precision (nm): 6.3, 6.8, 5.9, 6.7. **i**, 3D sizes of identified fibers by FWHM. N = 542 from 3 fields of view. Incubation with **6-HoeHESiR** (2.5 μM) for 10 min. Scale bar: 100 nm in **d** and **g**; 200 nm in **e** and **h**. Axial position represented by RGB color depth

coding.

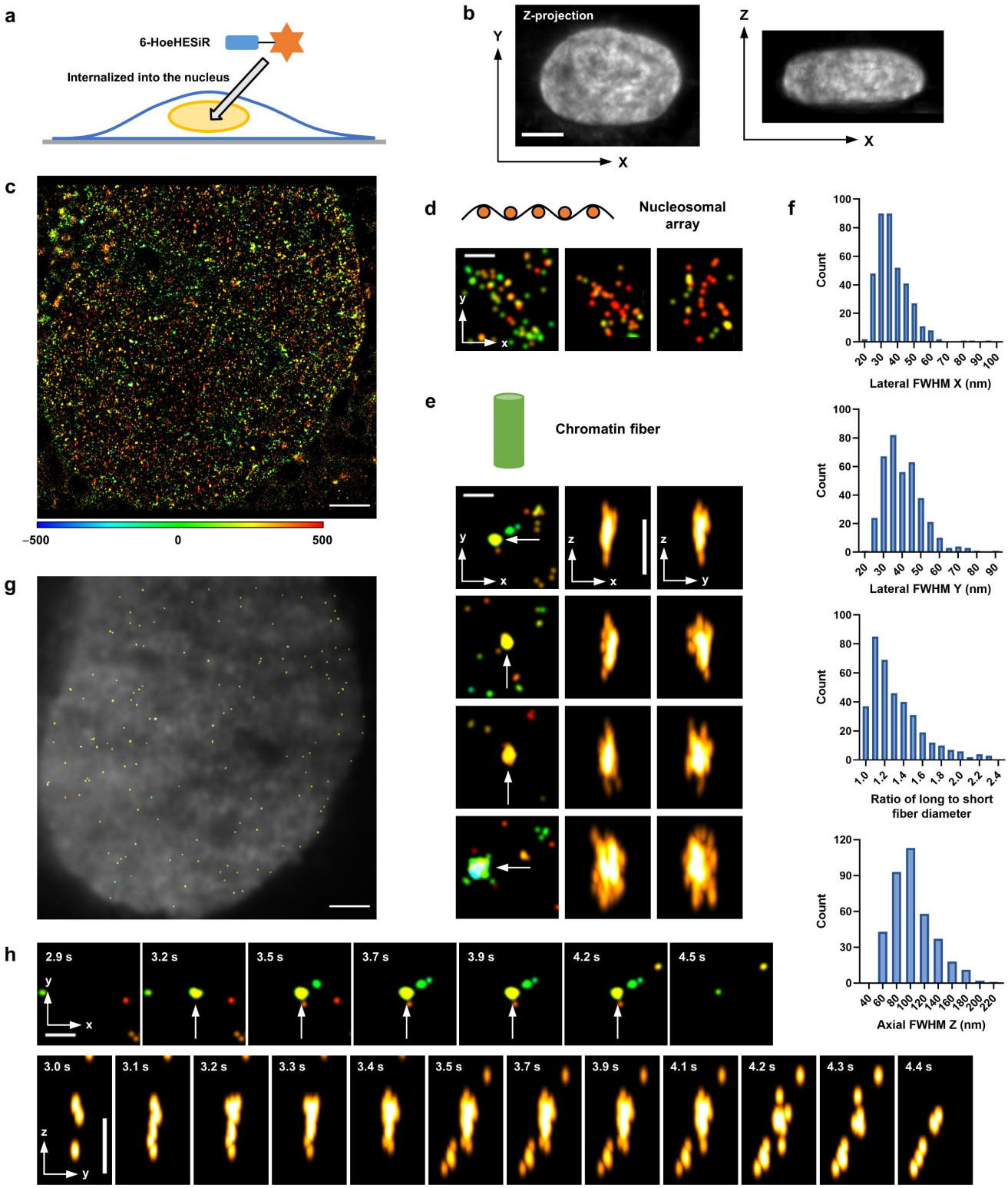

Fig. 4 Hierarchical chromatin structures in living HeLa cells. a, Schematic illustration of chromatin labeling with **6-HoeHESiR** (5 μM for 30 min). **b,** Images of a whole nucleus by light-sheet microscopy. **c**, Image of a nucleus. Reconstructed with 2,000 frames (17.7 ms/frame). **d**, Nucleosomal arrays. **e**,

Chromatin fibers. FWHM (x, y, z) in nm (from top to bottom): 30, 30, 107; 35, 42, 124; 34, 51, 102; 69, 51, 154. Localization precision (nm): 7.6, 6.8, 6.8, 9.5. **f**, 3D sizes of chromatin fibers by FWHM. N = 371 from 3 cells, identified in 500 frames. **g**, Distribution of chromatin fibers (identified in 500 frames). **h**, Fast dynamics of a chromatin fiber. Snapshots from Supplementary Videos 7 and 8 (Supplementary Information, video legends). Scale bar: 5 μm in **b**; 2 μm in **c** and **g**; 200 nm in **d**, **e** and **h**. Axial position represented by RGB color depth coding.

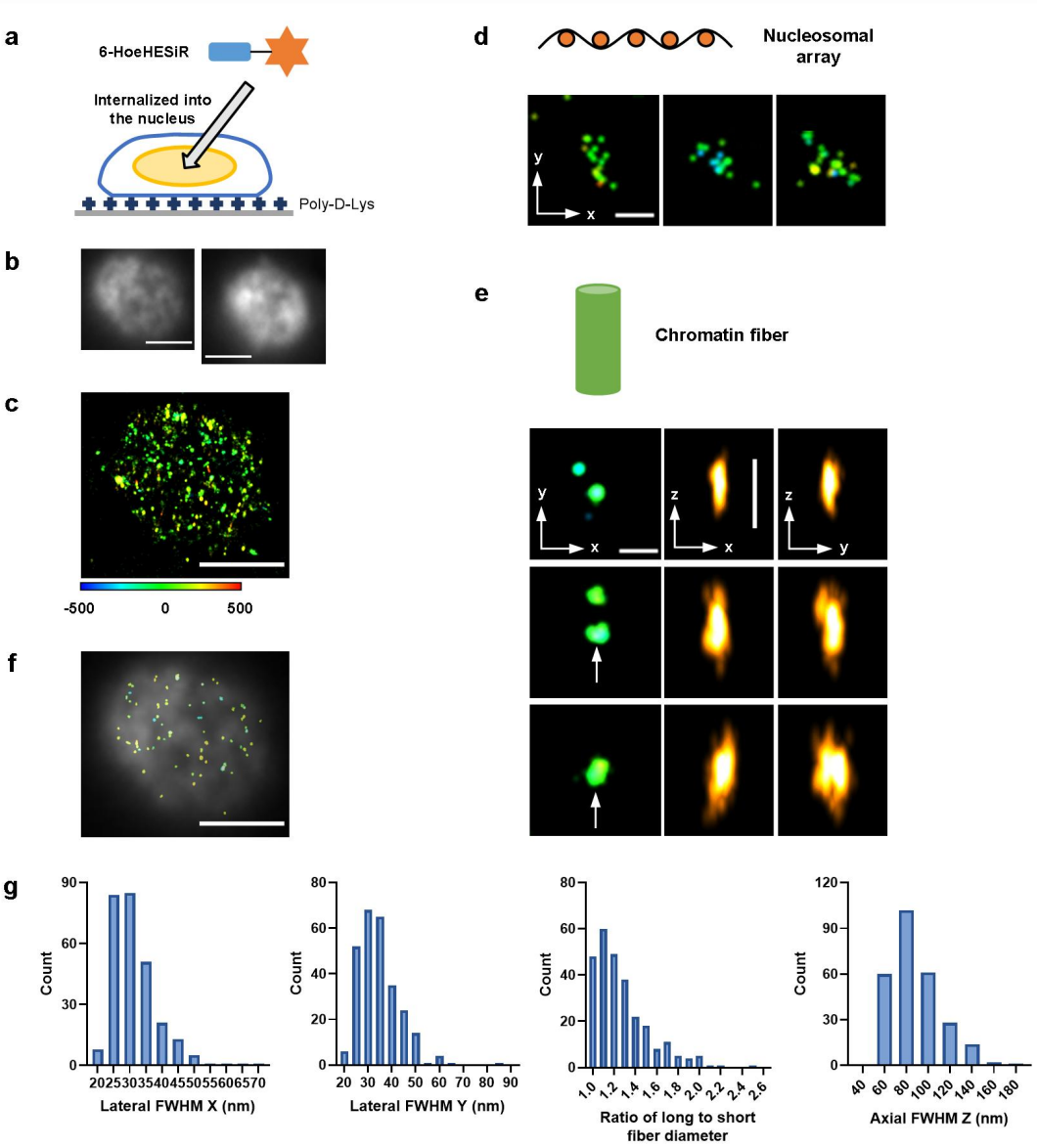

Fig. 5 Hierarchical chromatin structures in living chicken erythrocytes. a, Schematic illustration of chromatin labeling with **6-HoeHESiR** (0.5 μM for 10 min). **b,** Images of two nuclei obtained by widefield microscopy. **c**, Image of a nucleus. Reconstructed with 10,000 frames (17.7 ms/frame). **d**, Nucleosomal arrays. **e**, Chromatin fibers. FWHM (x, y, z) in nm (from top to bottom): 27, 29, 83; 37, 40, 124; 40, 62, 95. Localization precision (nm): 6.8, 6.9, 8.1. **f**, 3D sizes of chromatin fibers by FWHM. *N* = 271 from 3 cells, identified in 5,000 frames. **g**, Distribution of chromatin fibers (identified in 5,000 frames). Scale bar: 2 μm in **b**, **c** and **g**; 200 nm in **d** and **e**. Axial position represented by RGB color depth coding.

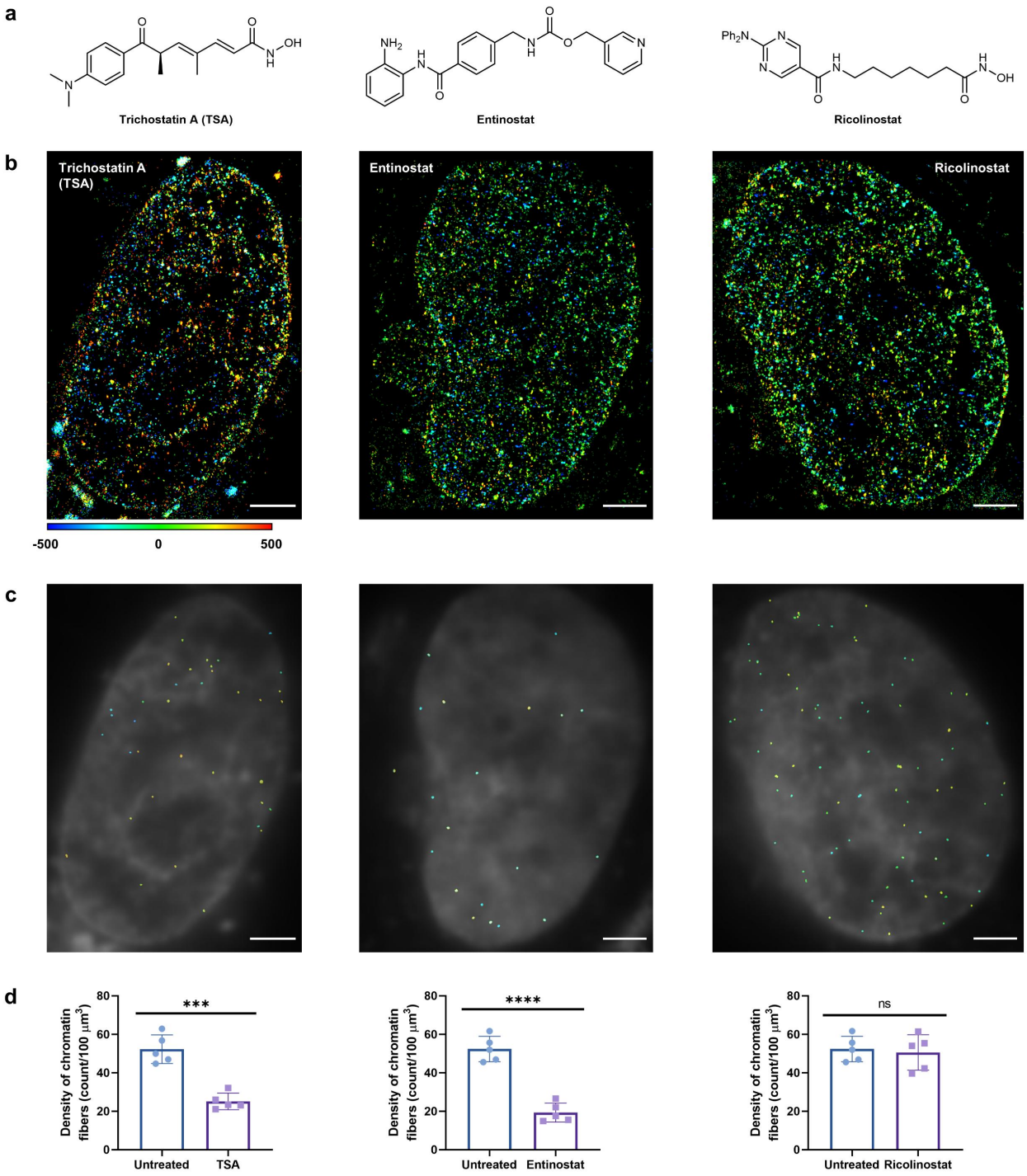

Fig. 6 Decompaction of chromatin fibers induced by HDAC inhibitors. **a**, Structures of small-molecule inhibitors of HDAC. **b**, Images of the nuclei in treated HeLa cells. Reconstructed with 2,000 frames (17.7 ms/frame). **c**, Distribution of chromatin fibers (identified in 500 frames). **d**, Density of chromatin fibers (identified in 500 frames). Data are individual values and mean ± s.d., $N = 5$. Statistical significance was determined by *t test* with $P = 0.0001$, <0.0001 and 0.7278 (from left to right).

406 The scale bar is 2 μm. Axial position represented by RGB color depth coding. Cells were treated with
407 TSA (200 nM), entinostat (2 μM), and ricolinostat (1 μM) for 20 h, respectively, and then incubated
408 with **6-HoeHESiR** (5 μM) for 30 min.

409

410

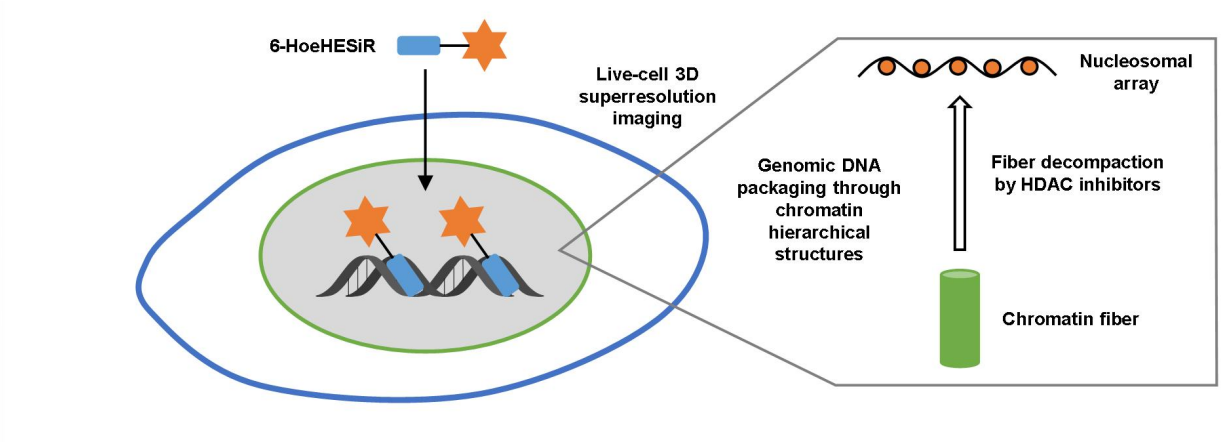

411

412 **Fig. 7** Schematic illustration of genomic DNA packaging via hierarchical chromatin structures in living

413 cells.

Supplementary Materials

Supplementary figures

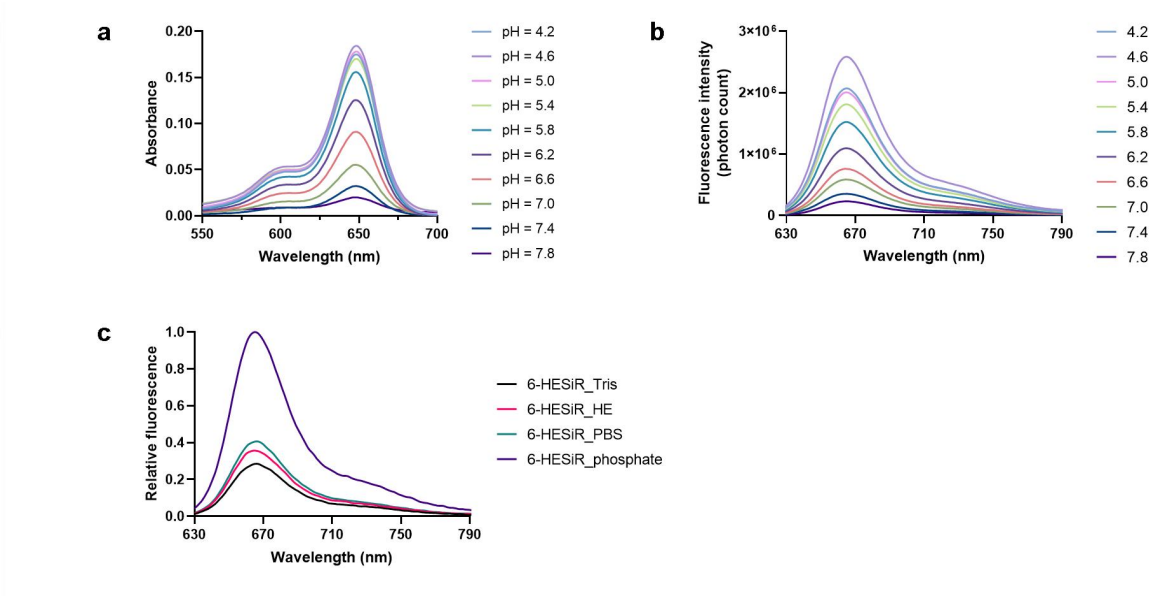

Supplementary Fig. 1 Photophysical properties of 6-HESiR. a, Absorption spectra of **6-HESiR** (2 μM) at various pH values in 0.1 M potassium phosphate buffer. **b**, Fluorescence emission spectra of **6-HESiR** (0.5 μM) at various pH values in 0.1 M potassium phosphate buffer. **c**, Fluorescence emission spectra of **6-HESiR** (2 μM) in aqueous buffers. Tris: 50 mM Tris-HCl, 100 mM NaCl (pH = 7.4). HE: 10 mM HEPES, 1 mM EDTA (pH = 7.5). PBS: 1× (pH = 7.4). Phosphate: 0.1 M potassium phosphate (pH = 7.4).

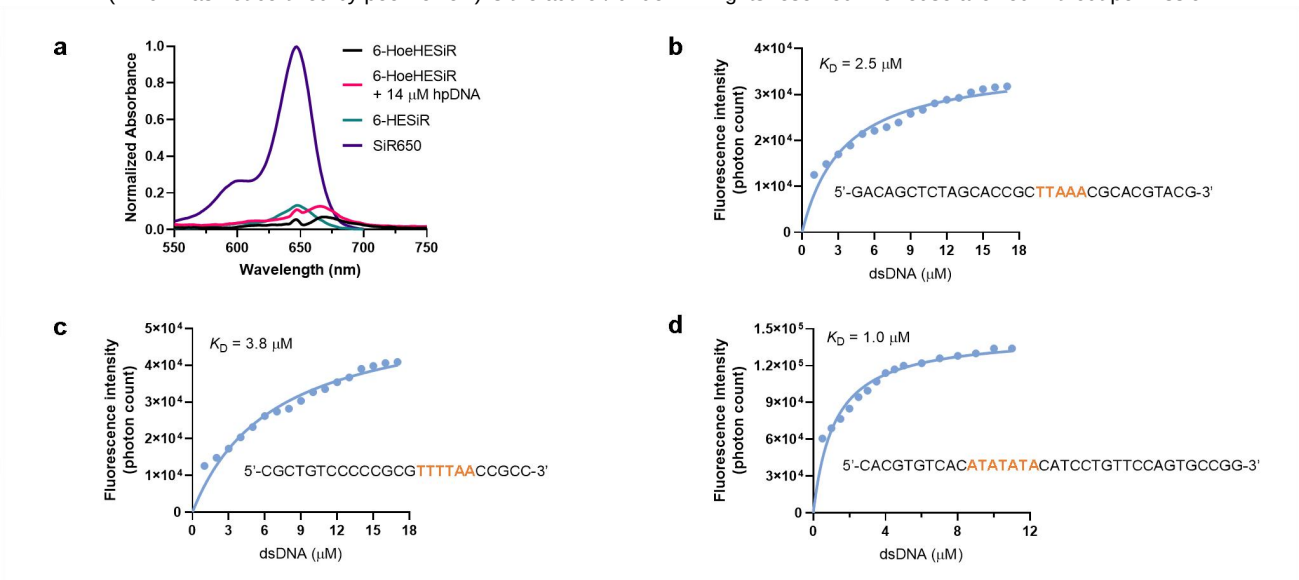

Supplementary Fig. 2 Fluorescence titration of 6-HoeHESiR. a, Absorbance of **6-HoeHESiR** (0.5 μM) in Tris-HCl saline buffer. Abs_{max} at 668 nm. **b-d**, Fluorescence titration with 0.5 μM **6-HoeHESiR** and dsDNA segments in the Tris-HCl saline buffer.

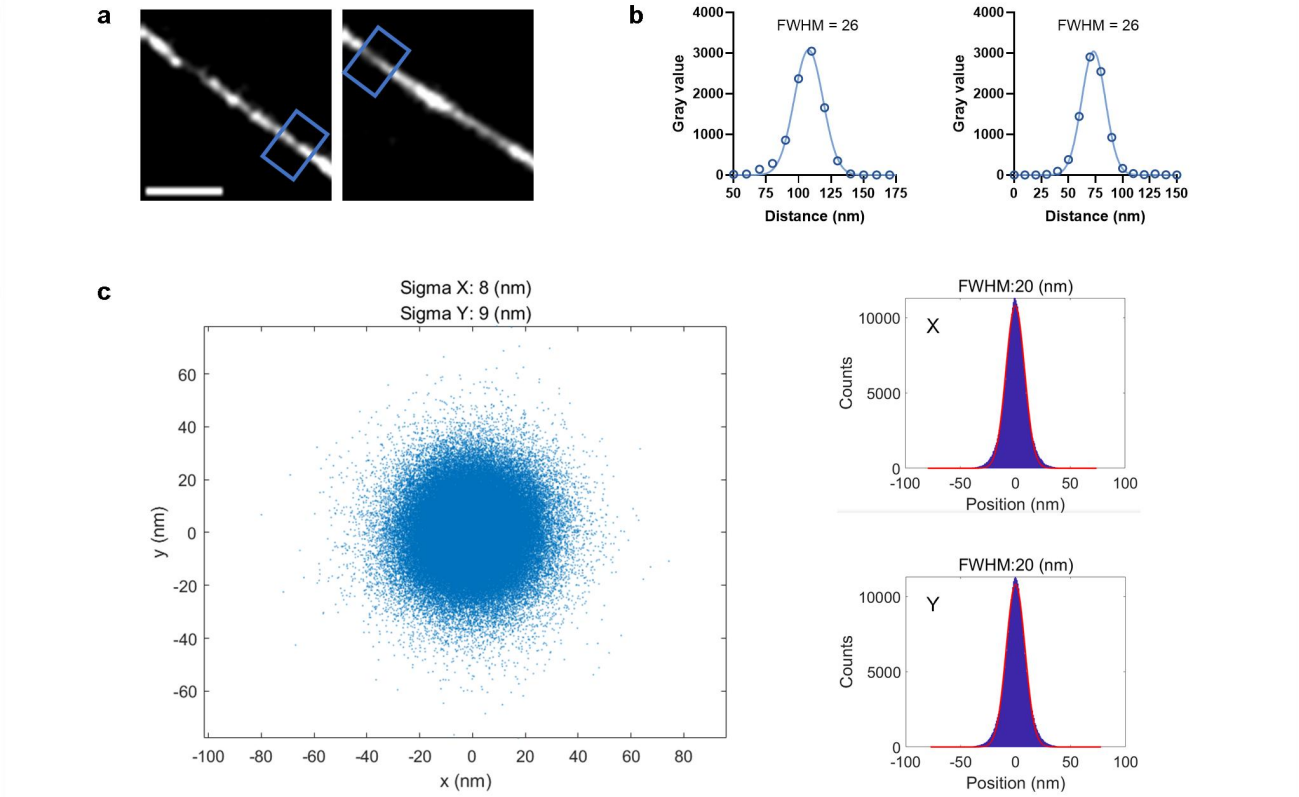

Supplementary Fig. 3 SMLM with lambda DNA. a, Reconstructed images of spin-coated λ-DNA. **b**, Line profiles for the boxed regions in **a** for obtaining FWHM values. **c**, Localization precision. Imaging performed with 100 nM **6-HoeHESiR**. Scale bar: 200 nm.

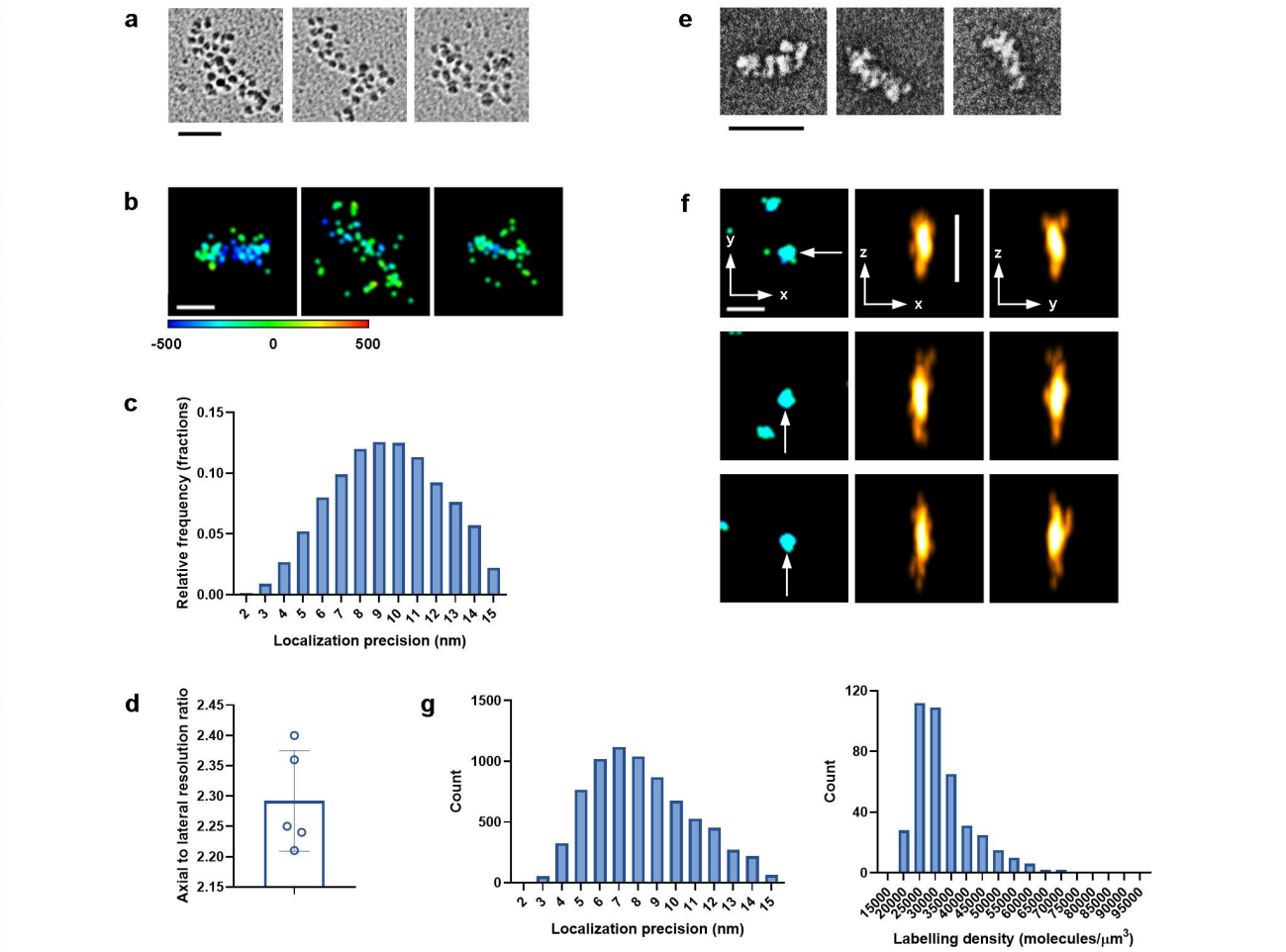

Supplementary Fig. 4 SMLM with *in vitro* reconstituted chromatin structures. a, EM images of 40×187-bp nucleosomal arrays (by metal-shadowing). **b**, Images of 40×187-bp nucleosomal arrays by 3D SMLM. **c**, Localization precision for 40 × 187-bp nucleosomal arrays. **d**, Ratio of axial resolution to lateral resolution for individual nucleosomes. Data are mean ± s.d., N = 5. **e**, EM images of 40×187-bp 30-nm chromatin fibers (negative staining). **f**, Images of 40×187-bp 30-nm fibers by 3D SMLM. FWHM (x, y, z) in nm: 30, 33, 96; 29, 30, 95; 27, 33, 107. Localization precision (nm): 6.2, 6.7, 6.6. From top to bottom. **g**, Localization precision and labeling density for identified 30-nm chromatin fibers. Incubation with **6-HoeHESiR** (2.5 μM) for 10 min. Scale bar: 100 nm in **a** and **e**; 200 nm in **b** and **f**. Axial position represented by RGB color depth coding.

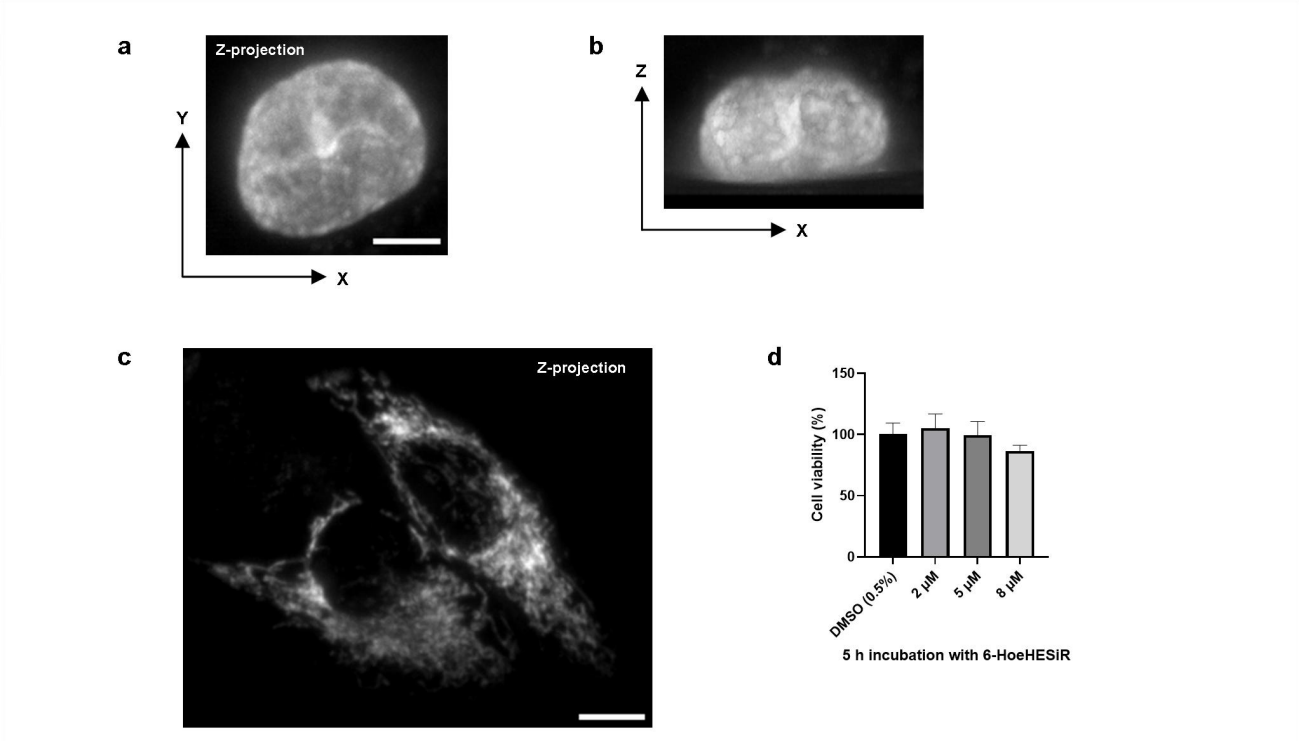

Supplementary Fig. 5 Light-sheet microscopy of living HeLa cells. a, The Z-projection image of the nucleus in a living HeLa cell. **b,** The XZ projection image of the same nucleus. **c**, The Z-projection image of living HeLa cells stained with **6-HESiR**. **d**, Cytotoxicity assay with **6-HoeHESiR**. *N* = 3, data are mean + SD. Incubation with **6-HoeHESiR** (5 µM) and **6-HESiR** (2 µM) for 30 min, respectively. Scale bar: 5 µm in **a** and **b**; 10 µm in **c**.

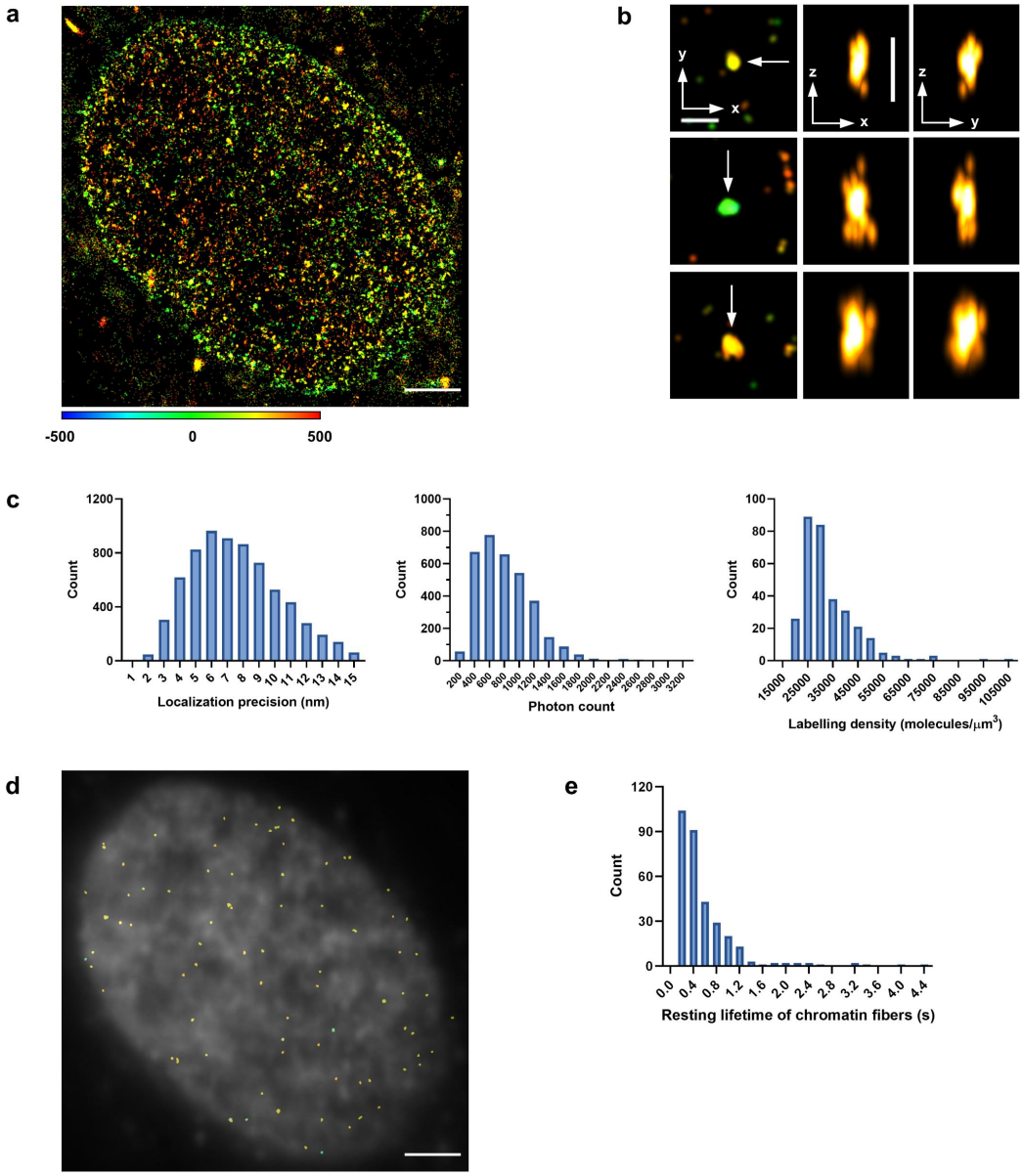

Supplementary Fig. 6 Chromatin fibers in living HeLa cells. a, The image of a nucleus. Reconstructed from 2,000 frames (17.7 ms/frame). **b**, High-order chromatin fibers. FWHM (x, y, z) in nm (from top to bottom.): 31, 34, 94; 44, 35, 116; 45, 50, 103. Localization precision (nm): 7, 7.2, 9.1. **c**, Localization precision, photon count and labeling density for identified fibers in 500 frames. **d**, The distribution of chromatin fibers (identified in 500 frames). **e**, Lifetime of identified fibers in 500 frames. Incubation with **6-HoeHESiR** (5 μM) for 30 min. Scale bar: 2 μm in **a** and **d**; 200 nm in **b**. Axial position represented by RGB color depth coding.

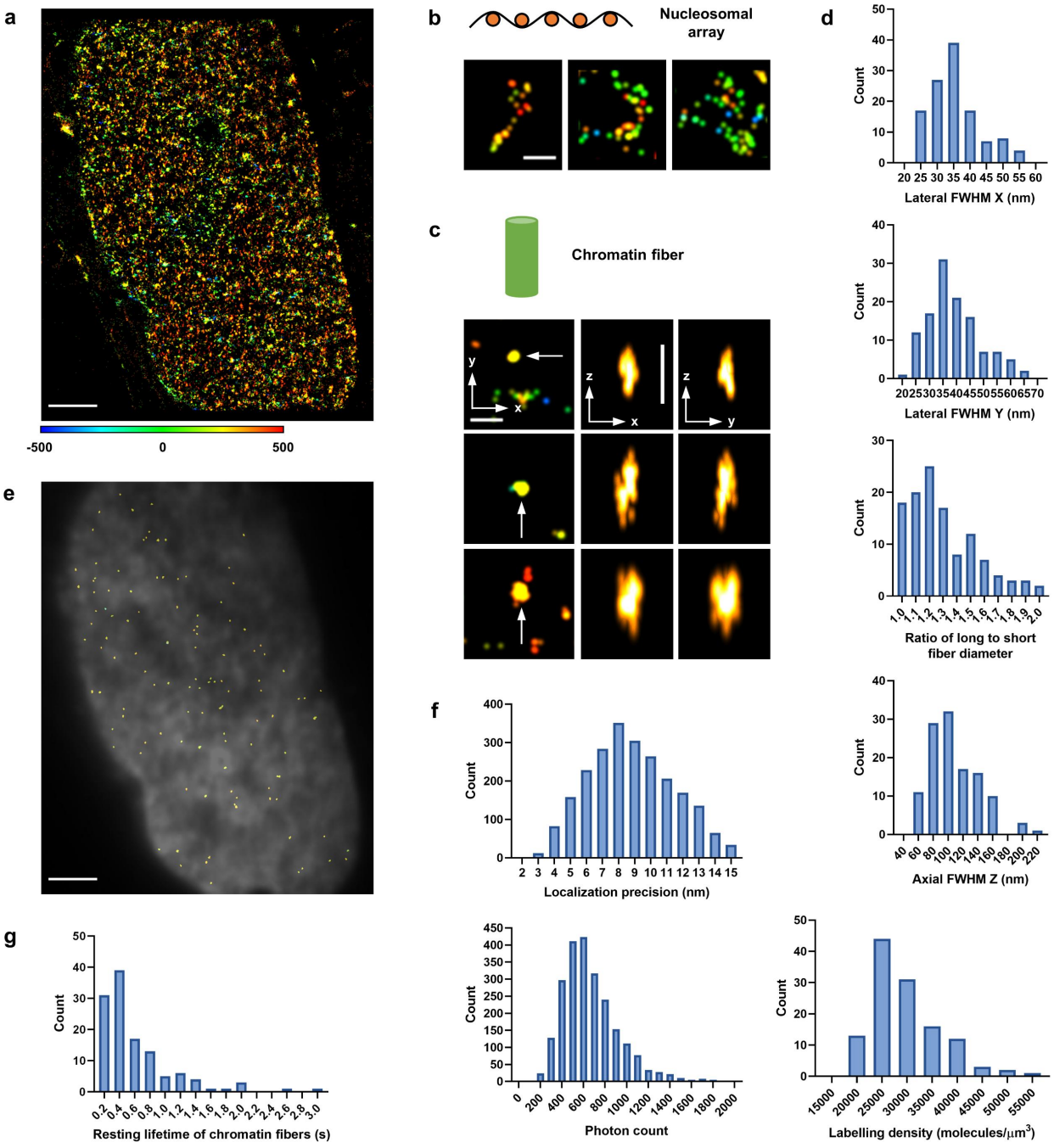

Supplementary Fig. 7 Hierarchical chromatin structures in a living HeLa cell with reduced phototoxicity. a, The image of a nucleus. Reconstructed from 2,000 frames (17.7 ms/frame). **b**, Images of nucleosomal arrays. **c**, Chromatin fibers. FWHM (x, y, z) in nm (from top to bottom): 31, 33, 95; 42, 36, 130; 47, 62, 112. Localization precision (nm): 6.8, 7.2, 8.9. **d**, 3D sizes of identified fibers in 500 frames. N = 119. **e**, The distribution of chromatin fibers (identified in 500 frames). **f**,

Localization precision, photon count and labeling density for identified fibers in 500 frames. **g**, Lifetime of identified fibers in 500 frames. Incubation with **6-HoeHESiR** (5 μM) for 30 min. Scale bar: 2 μm in **a** and **e**; 200 nm in **b** and **c**. Axial position represented by RGB color depth coding.

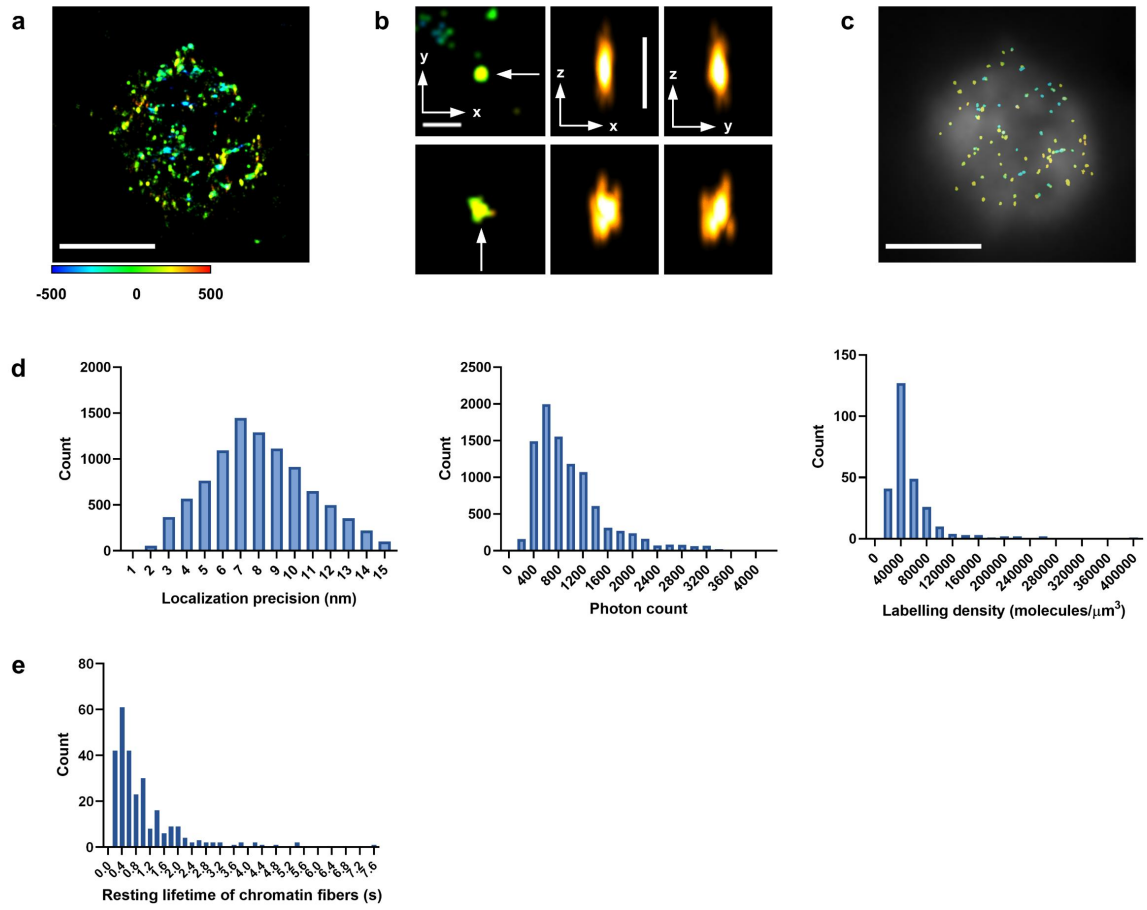

Supplementary Fig. 8 High-order chromatin fibers in living chicken erythrocytes. a, The image of a nucleus. Reconstructed with 5,000 frames (17.7 ms/frame). **b**, Chromatin fibers. FWHM (x, y, z) in nm (upper, lower): 25, 33, 84; 51, 47, 94. Localization precision (nm): 7.4, 8.5. **c**, The distribution of chromatin fibers (data from 5,000 frames). **d**, Localization precision, photon count and labeling density for identified fibers in 5,000 frames. **e**, Lifetime of identified fibers in 5,000 frames. Incubation with **6-HoeHESiR** (0.5 μM) for 10 min. Scale bar: 2 μm in **a** and **c**; 200 nm in **b**. Axial position represented by RGB color depth coding.

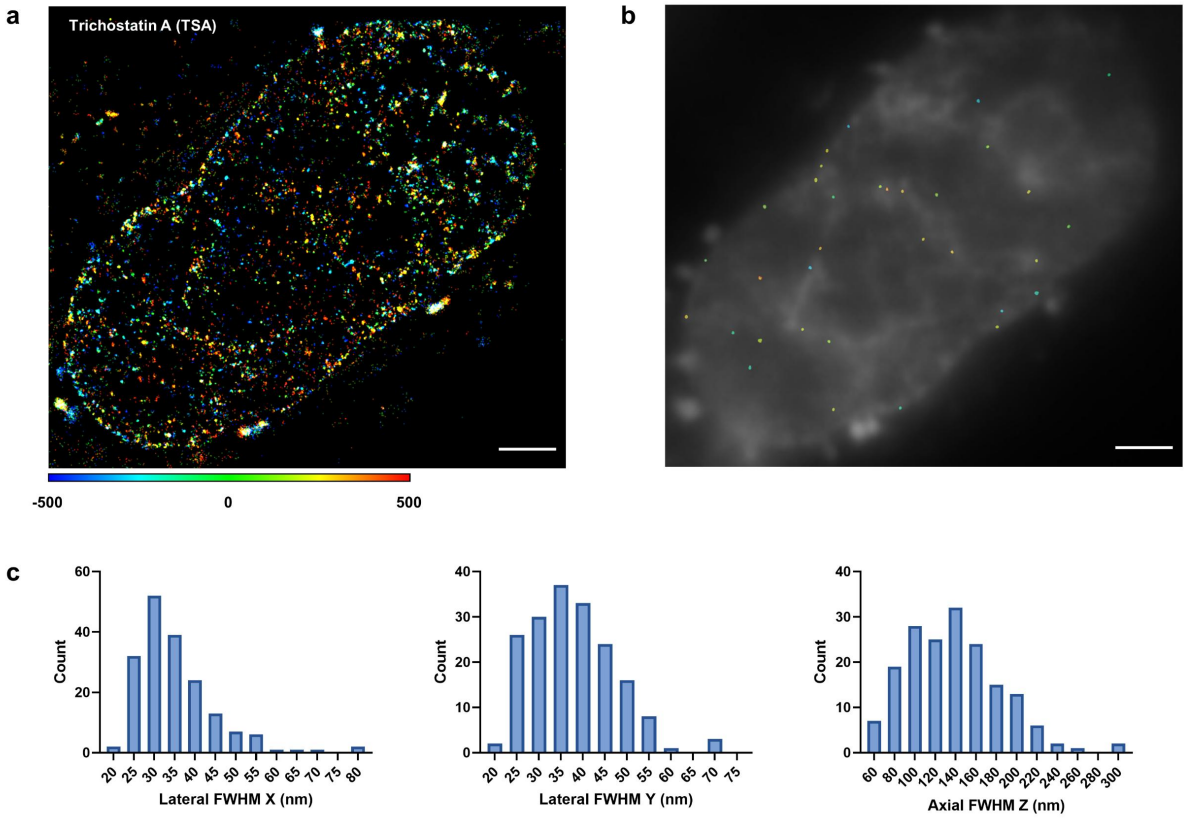

Supplementary Fig. 9 Treatment with trichostatin A. a, The nucleus of a treated HeLa cell. Reconstructed with 2,000 frames (17.7 ms/frame). **b**, The distribution of chromatin fibers (identified in 500 frames). **c**, 3D sizes of chromatin fibers from 5 cells. N = 180. Identified in 500 frames. Incubation with **6-HoeHESiR** (5 μM) for 30 min. Scale bar is 2 μm. Axial position represented by RGB color depth coding.

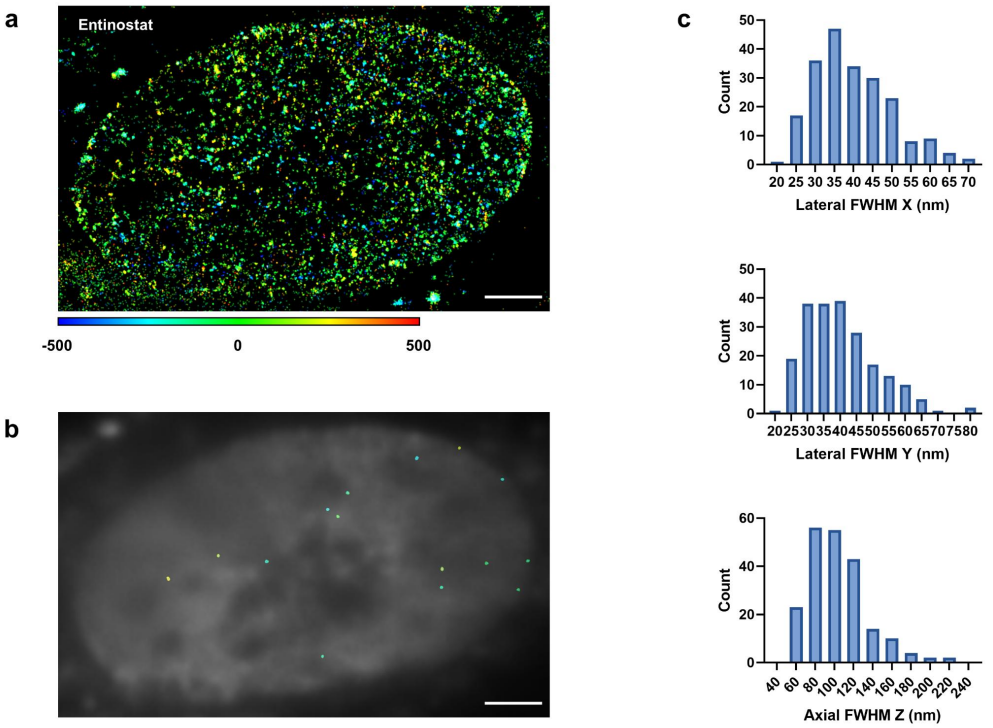

Supplementary Fig. 10 Treatment with entinostat. a, The nucleus of a treated HeLa cell. Reconstructed with 2,000 frames (17.7 ms/frame). **b**, The distribution of chromatin fibers (identified in 500 frames). **c**, 3D sizes of chromatin fibers from 5 cells. N = 211. Identified in 500 frames. Incubation with **6-HoeHESiR** (5 μM) for 30 min. Scale bar is 2 μm. Axial position represented by RGB color depth coding.

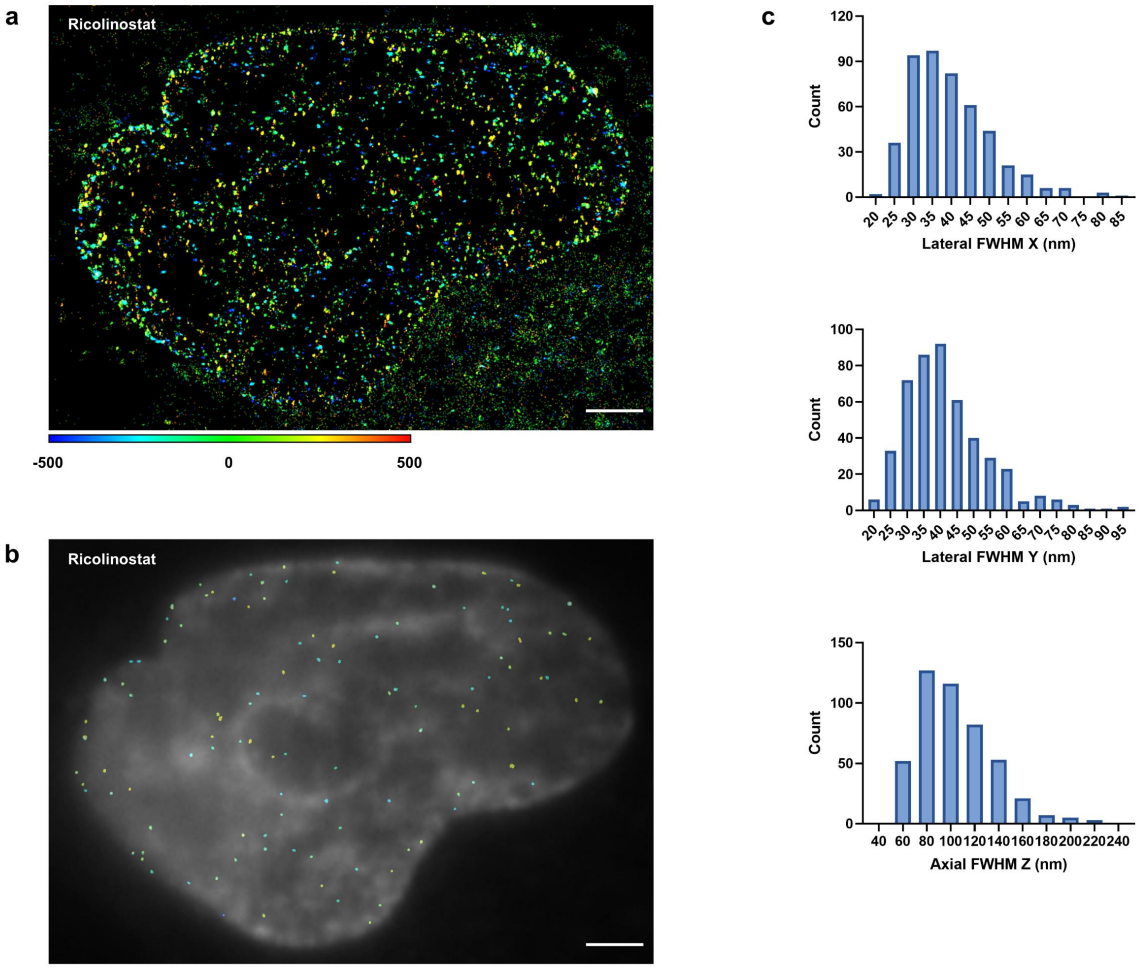

Supplementary Fig. 11 Treatment with ricolinostat. a, The nucleus of a treated HeLa cell. Reconstructed with 2,000 frames (17.7 ms/frame). **b**, The distribution of chromatin fibers (identified in 500 frames). **c**, 3D sizes of chromatin fibers from 5 cells. N = 468. Identified in 500 frames. Incubation with **6-HoeHESiR** (5 μM) for 30 min. Scale bar is 2 μm. Axial position represented by RGB color depth coding.

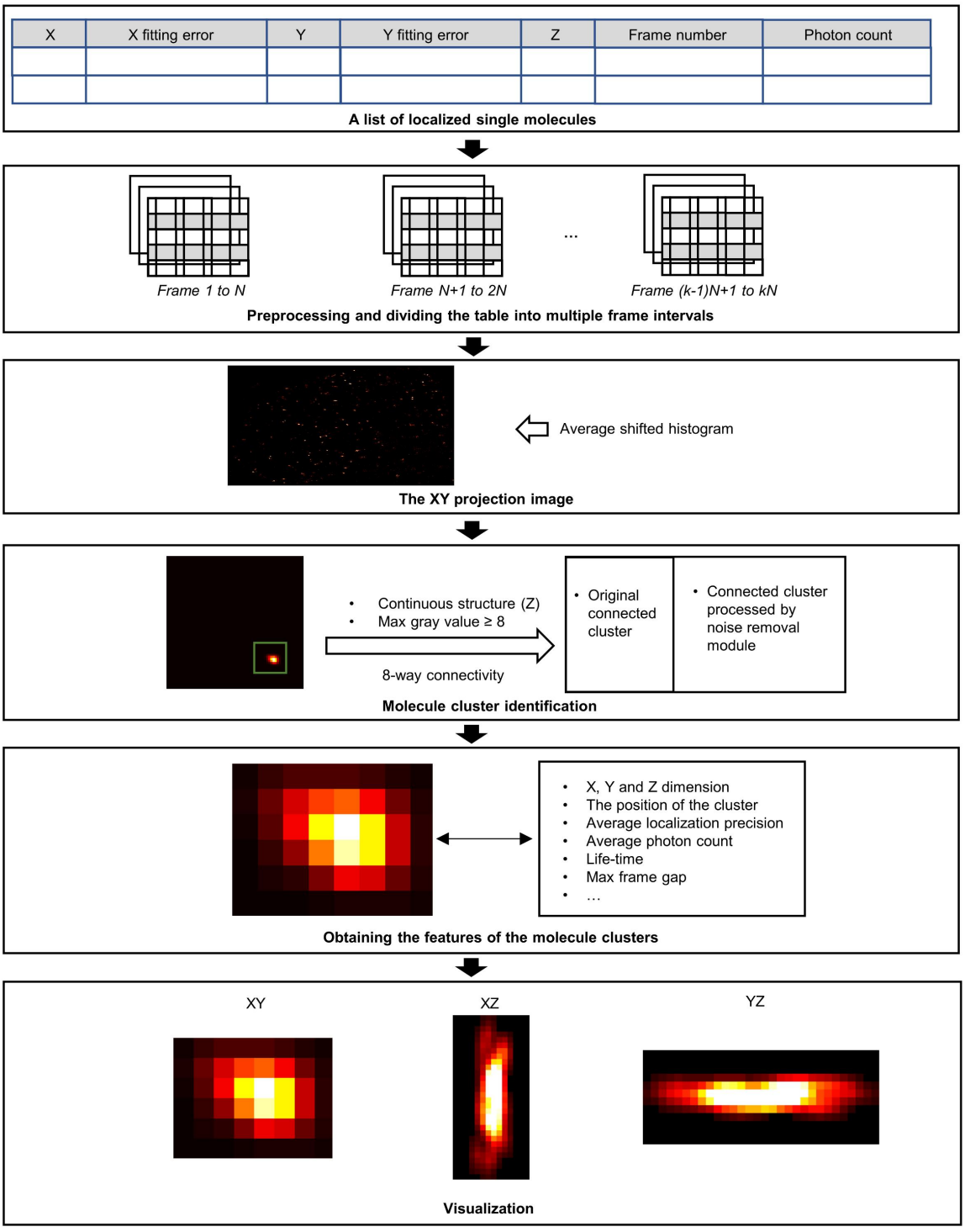

Supplementary Fig. 12 The flowchart of the analysis of molecular clusters for identification of chromatin fibers.

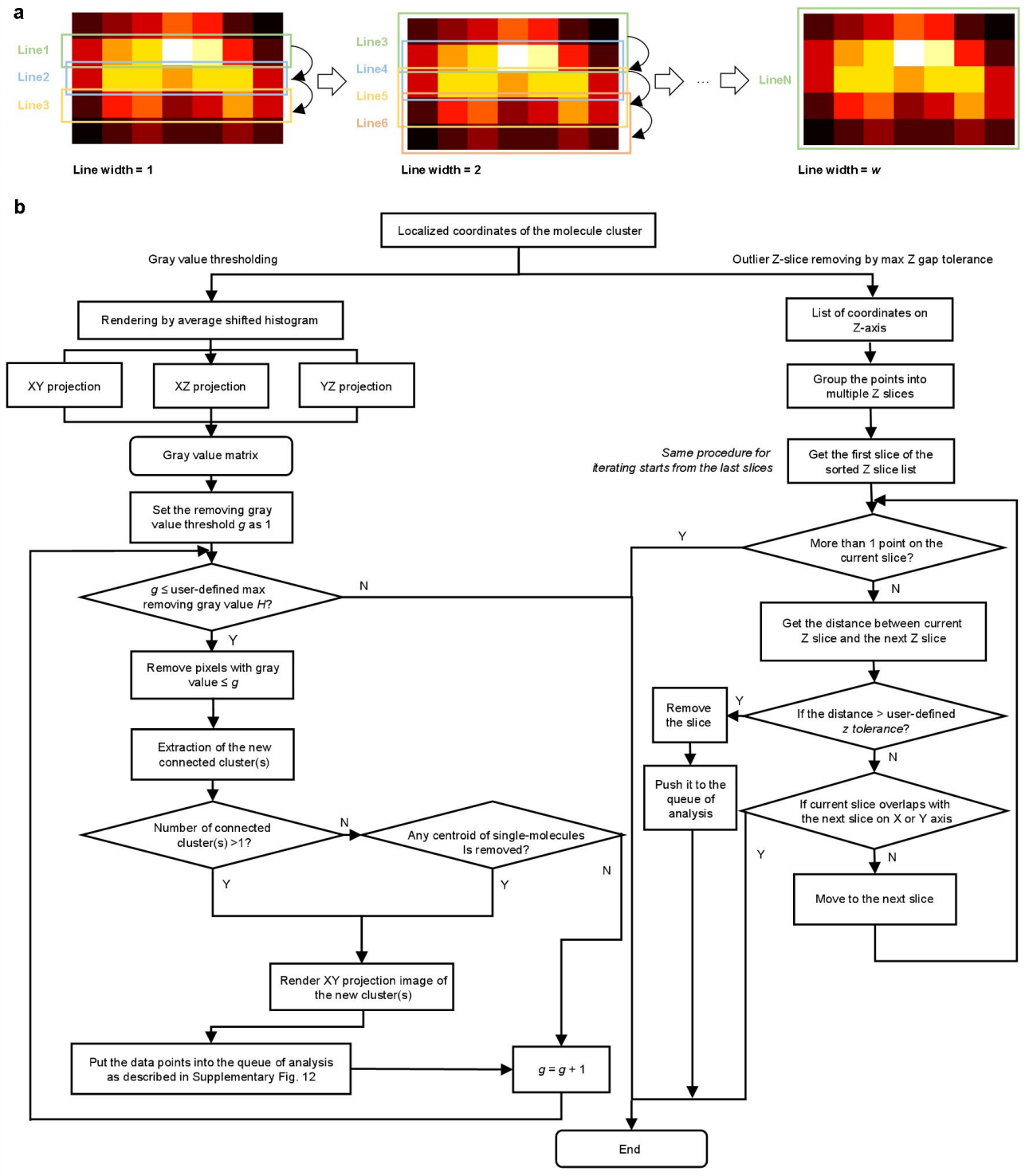

Supplementary Fig. 13 Chromatin fiber analysis program. a, The demonstration of the moving line strategy for estimating X dimension of molecular clusters. **b**, The flowchart of the noise removal module, which consists of two submodules: gray value thresholding and outlier Z slice removing by max Z gap tolerance. *g* ranges from 1 to the user-defined max threshold *H*.

Supplementary video legends

1. Self-blinking of **6-HoeHESiR** in a 3D SMLM experiment of *in vitro* reconstituted 30-nm chromatin fibers. Scale bar: 2 μm. 950 W/cm^2 laser intensity at 656 nm. Camera exposure at 17.7 ms/frame.
2. 3D rotation of an *in vitro* reconstituted chromatin fiber in Fig. 3h. Scale bar: 200 nm
3. 3D rotation of another *in vitro* reconstituted chromatin fiber in Fig. 3h. Scale bar: 200 nm
4. Self-blinking of **6-HoeHESiR** in a 3D SMLM experiment of a living HeLa cell. Scale bar: 2 μm. 3.2 kW/cm^2 laser intensity at 656 nm. Camera exposure at 17.7 ms/frame.
5. 3D rotation of a chromatin fiber in a HeLa cell in Fig. 4e.
6. 3D rotation of another chromatin fiber in a HeLa cell in Fig. 4e.
7. Time-lapse video (z-projection) of dynamic chromatin structures in a living HeLa cell. 56 frames per image. 5 frames per sliding window. Scale bar: 2 μm. 3.2 kW/cm^2 laser intensity at 656 nm. Camera exposure at 17.7 ms/frame. Axial position is represented by RGB color depth coding.
8. Time-lapse video (yz-projection) of a chromatin fiber in Fig. 4e. 56 frames per image. 5 frames per sliding window. Scale bar: 200 nm. 3.2 kW/cm^2 laser intensity at 656 nm. Camera exposure at 17.7 ms/frame.
9. Time-lapse video (z-projection) of chromatin dynamics in a living HeLa cell with reduced phototoxicity. 56 frames per image. 5 frames per sliding window. Scale bar: 2 μm. 950 W/cm^2 laser intensity at 656 nm. Camera exposure at 17.7 ms/frame. Axial position is represented by RGB color depth coding.
10. Self-blinking of **6-HoeHESiR** in a 3D SMLM experiment of a living chicken erythrocyte. Scale bar: 2 μm. 950 W/cm^2 laser intensity at 656 nm. Camera exposure at 17.7 ms/frame.
11. 3D rotation of a chromatin fiber in a chicken erythrocyte in Fig. 5e. Scale bar: 200 nm
12. 3D rotation of another chromatin fiber of a chicken erythrocyte in Fig. 5e. Scale bar: 200 nm

13. Time-lapse video (z-projection) of chromatin dynamics in a living chicken erythrocyte with reduced phototoxicity. 56 frames per image. 5 frames per sliding window. Scale bar: 2 μm. 950 W/cm^2 laser intensity at 656 nm. Camera exposure at 17.7 ms/frame. Axial position is represented by RGB color depth coding.

Chemical synthesis and characterization

General information

NMR spectra were acquired on Bruker 400 and 500 MHz spectrometers. High resolution mass spectra were acquired on Bruker maXis II and Thermo Scientific DFS. Preparative reverse phase HPLC was performed on a Waters preparative HPLC system with a C18 reverse phase column. All chemicals and reagents were purchased from commercial sources and used without further purification. Dess-Martin periodinane (DMP), dry *N*,*N*-diisopropylethylamine (DIEA), triethylamine and trifluoroacetic acid (TFA) were purchased from Energy Chemical. DIEA was purchased from TCI. $ClPh_3PCH_2OMe$ and Hoechst 33258 were purchased from J&K. NaHMDS was purchased from Alfa Aesar. $NaBH_4$ was purchased from Lancaster Synthesis. Chloromethyl methyl ether (MOMCl) was purchased from Sigma Aldrich. *s*-BuLi was purchased from Infinity Scientific. 4-Nitrophenyl chloroformate was purchased from Apollo Scientific. All solvents were either AR or HPLC grade. Dry dichloromethane (CH_2Cl_2) and dry tetrahydrofuran (THF) were obtained from a solvent purification system. Dry dimethylformamide (DMF) was purchased from Energy Chemical. Deuterated solvents $CDCl_3$ and CD_3OD for NMR experiments were purchased from Cambridge Isotope Laboratories.

Synthetic route of 6-HESiR

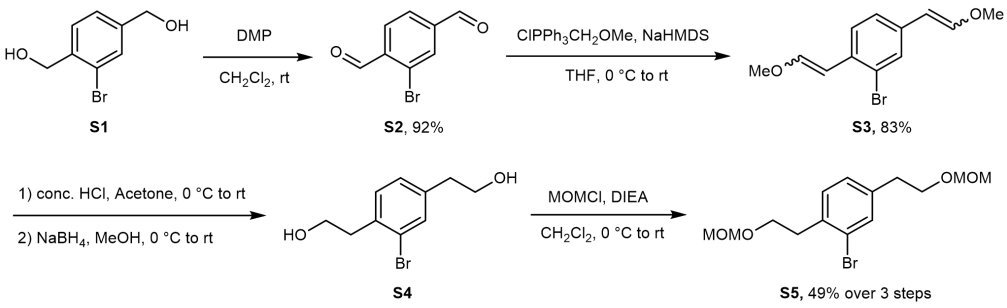

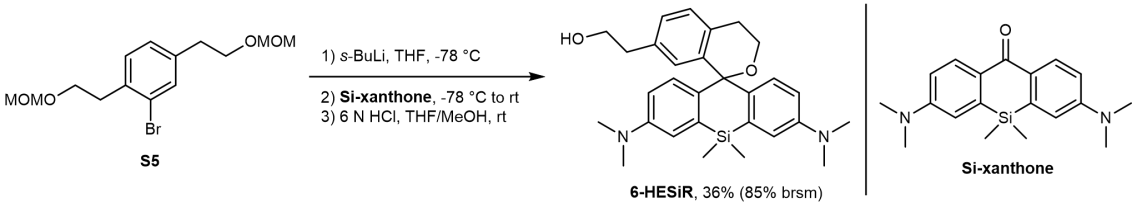

Procedures for making 6-HESiR

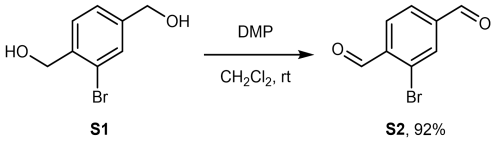

S1[1] (0.868 g, 4 mmol) and Dess-Martin periodinane (3.64 g, 8.4 mmol) were added to a 100 mL round-bottom flask, followed by CH_2Cl_2 (40 mL). The mixture was stirred at room temperature for 3 h. The milky suspension was quenched by saturated $NaHCO_3$ and extracted with CH_2Cl_2 three times. The combined organic phase was dried over $MgSO_4$, filtered and concentrated. The crude product was purified by flash column chromatography (10% to 20% ethyl acetate/hexane) to give the known compound **S2**[2] as a white solid (0.788 g, 3.7 mmol, 92% yield).

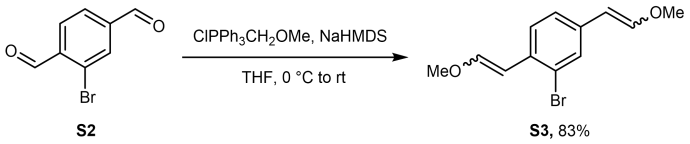

To a 100 mL round-bottom flask with $ClPh_3PCH_2OMe$ (1.58 g, 4.49 mmol, dried before reaction) under argon (Ar) was added THF (anhydrous, 7 mL). The flask was cooled in an ice/water bath with stirring under Ar. 2 M THF solution of NaHMDS (2.25 mL, 4.5 mmol) was added at 0 °C and the resulting mixture was stirred at the same temperature for 1 h. **S2** (0.318 g, 1.49 mmol) dissolved in THF (anhydrous, 4 mL) was transferred to the first flask. Bath was removed and the reaction mixture was warmed to rt and stirred overnight. On the next day, the reaction was quenched with sat. NH_4Cl, diluted with ethyl acetate (EA) and water, and extracted with EA three times. The combined organic phase was dried over $MgSO_4$, filtered and concentrated. The crude product was purified by flash

column chromatography (15% CH_2Cl_2/hexane, then 5% EA/hexane) to give **S3** as a light-yellow oil (0.332 g, 1.23 mmol, 83% yield). Due to instability of **S3**, only ^{1}H NMR spectrum was acquired. Due to complexity of the spectrum caused by two pairs of E/Z isomers, only integral ratios are provided. ^{1}H NMR (500 MHz, $CDCl_3$) δ 7.97–7.93, 7.81–7.78, 7.41–7.36, 7.25–7.22, 7.11–7.06 (3H, aromatic protons), 7.04–6.95, 6.22–6.20, 6.14–6.12, 6.09–6.04, 5.72–5.69, 5.59–5.56, 5.13–5.11 (4H, vinylic protons), 3.79–3.77, 3.72, 3.68 (6H, protons of two methyl groups).

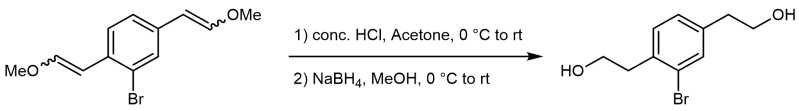

S3 **S4**

S3 (0.332 g, 1.23 mmol) was dissolved with acetone (13 mL) in a 100 mL round-bottom flask and the solution was cooled in an ice/water bath. Concentrated HCl (1 mL) was added to the solution and the mixture was stirred for 30 min at 0 °C. Then bath was removed, and the reaction was warmed to room temperature and stirred for another 1.5 h. The reaction was quenched with sat. $NaHCO_3$ and extracted three times with EA. The combined organic phase was washed with brine, dried over $MgSO_4$, filtered, and concentrated. Then methanol (14 mL) was added, and the round-bottom flask was cooled in an ice/water bath with stirring. $NaBH_4$ (0.375 g, 12.3 mmol) was added carefully (gas evolution) at 0 °C. The reaction mixture was stirred at the same temperature for 30 min. Then bath was removed, and the reaction was warmed to room temperature and stirred overnight (reaction time unoptimized). On the next day, saturated $NaHCO_3$ was added and EA was used to extract the mixture three times. The combined organic phase was washed with brine, dried over $MgSO_4$, filtered, and concentrated. The crude product was purified by flash column chromatography (2% to 4% MeOH/CH_2Cl_2) to give **S4** as a light-yellow viscous oil mixed with inseparable impurities, which was used for the next step without further purification. The crude product could also be directly used for the next step without flash column chromatography.

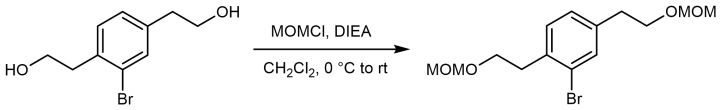

S4 **S5,** 49% over 3 steps

To a 100 mL round-bottom flask with **S4** under Ar were added dry CH_2Cl_2 (12 mL) and dry DIEA (1.26 mL, 7.38 mmol) sequentially. The flask was cooled in an ice/water bath with stirring under Ar. MOMCl (0.52 mL, 6.15 mmol) was added dropwise at 0 °C. The reaction mixture was gradually warmed to room temperature and stirred overnight (reaction time unoptimized). On the next day, the reaction was quenched with water and extracted three times with CH_2Cl_2. The combined organic phase was dried over $MgSO_4$, filtered and concentrated. The crude product was purified by flash column chromatography (5% to 10% EA/hexane) to give **S5** as a colorless oil (200 mg, 0.6 mmol, 49% yield over 3 steps). ^{1}H NMR (500 MHz, $CDCl_3$) δ 7.44 (d, J = 1.4 Hz, 1H), 7.20 (d, J = 7.8 Hz, 1H), 7.11 (dd, J = 7.8, 1.4 Hz, 1H), 4.62 (s, 2H), 4.61 (s, 2H), 3.75 (t, J = 7.5 Hz, 2H), 3.74 (t, J = 7.3 Hz, 2H), 3.31 (s, 3H), 3.30 (s, 3H), 3.02 (t, J = 7.1 Hz, 2H), 2.85 (t, J = 6.8 Hz, 2H); ^{13}C NMR (100 MHz, $CDCl_3$) δ 139.5, 136.1, 133.4, 131.2, 128.3, 124.8, 96.7, 96.6, 68.3, 67.0, 55.54, 55.48, 36.4, 35.7; HRMS (EI): calcd for $C_{14}H_{21}BrO_4$ (M^+): 332.0623, 334.0603, found: 332.0613, 334.0600.

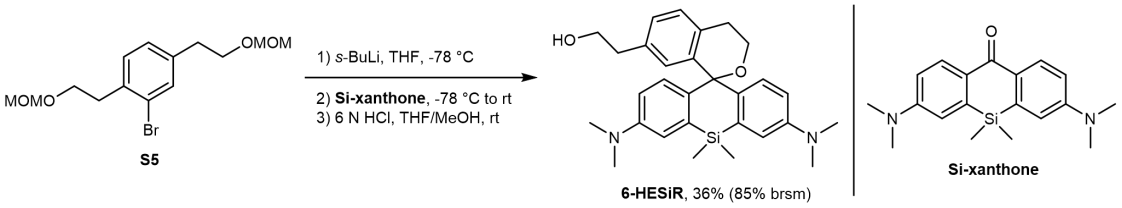

S5 **6-HESiR**, 36% (85% brsm) **Si-xanthone**

To a 100 mL round-bottom flask with **S5** (0.31 g, 0.93 mmol) under Ar was added THF (anhydrous, 4 mL). The solution was cooled in a dry ice/acetone bath with stirring. *s*-BuLi solution (0.97 mL, 0.96 M in hexane) was added dropwise at −78 °C and the resulting mixture was stirred for 3.5 h at the same temperature under Ar. Si-xanthone[3] (0.32 g, 0.99 mmol) was suspended in dry THF (sonication applied) and transferred to the first flask under Ar. This suspension/transfer operation was repeated several times (11 mL anhydrous THF in total) and THF (anhydrous, 2 mL) was added

at the end to rinse the remaining residue. Upon completed transfer of Si-xanthone, the cold bath was removed, and the reaction was warmed to room temperature and stirred overnight (reaction time unoptimized). The flask was wrapped with aluminum foil to shield it from light. On the next day, the reaction was quenched with saturated NH_4Cl and a small amount of 1 N HCl. The resulting deep blue mixture was diluted with water and extracted four times with CH_2Cl_2. The combined organic phase was dried over Na_2SO_4, filtered and concentrated. Then THF (4 mL) and MeOH (4 mL) were added, followed by 6 N HCl (10 mL). The reaction mixture was stirred at room temperature overnight (reaction time unoptimized). On the next day, the reaction mixture was diluted with water and quenched with solid Na_2CO_3 carefully (gas evolution). EA was added and the mixture was stirred vigorously until the deep blue color faded. Then the mixture was extracted with EA four times. The combined organic phase was washed with brine, dried over $MgSO_4$, filtered, and concentrated. The crude product was purified by flash column chromatography (20% EA/20% CH_2Cl_2/1% triethylamine/hexane to 50% EA/20% CH_2Cl_2/1% triethylamine/hexane) to give **6-HESiR** as a light blue foam (160 mg, 0.338 mmol, 36% yield). Based on recovered Si-xanthone (190 mg), the yield of **6-HESiR** based on recovered starting material (brsm) was 85%. ^{1}H NMR (500 MHz, $CDCl_3$) δ 7.18 (d, J = 7.8 Hz, 1H), 7.14 (d, J = 7.8 Hz, 1H), 7.06 (s, 2H), 6.89 (s, 1H), 6.72 (d, J = 8.8 Hz, 2H), 6.50 (d, J = 8.7 Hz, 2H), 3.76 (t, J = 6.6 Hz, 2H), 3.58 (t, J = 5.2 Hz, 2H), 2.93 (s, 12H), 2.81 (t, J = 5.2 Hz, 2H), 2.76 (t, J = 6.5 Hz, 2H), 0.62 (s, 3H), 0.49 (s, 3H); ^{13}C NMR (125 MHz, $CDCl_3$) δ 148.8, 139.3, 139.0, 138.3, 134.7, 134.6, 131.4, 130.5, 129.1, 127.3, 117.7, 112.1, 82.2, 63.9, 59.2, 40.6, 39.0, 29.2, 1.2, –2.7; HRMS (ESI): calcd for $C_{29}H_{36}N_2O_2Si$ ($[M + H]^+$): 473.2619, found: 473.2622.

Synthetic route of 6-HoeHESiR

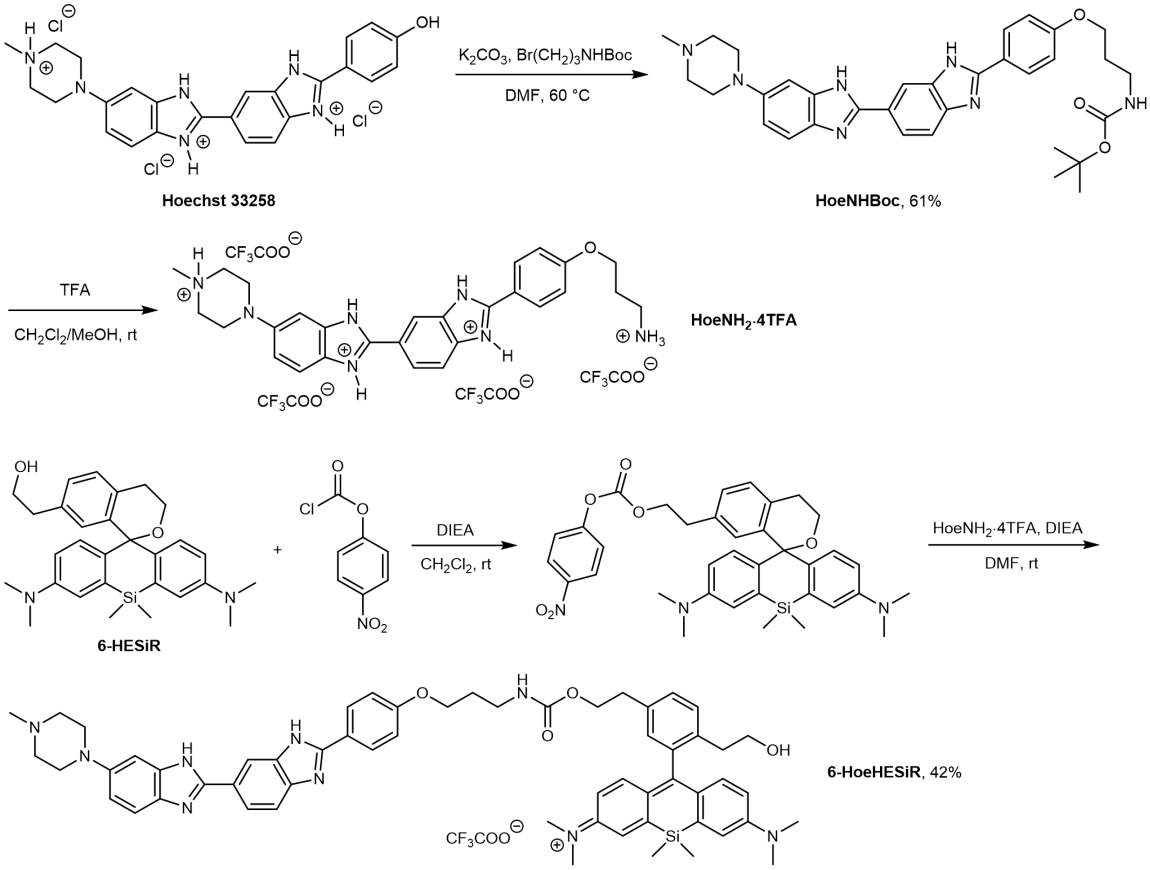

Procedures for preparation of 6-HoeHESiR

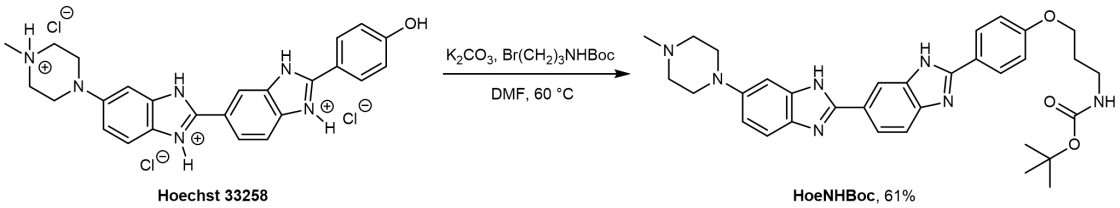

To a 25 mL round-bottom flask with **Hoechst 33258** (63 mg, 0.12 mmol), $Br(CH_2)_3NHBoc$[4] (56 mg, 0.236 mmol) and K_2CO_3 (49 mg, 0.354 mmol) was added DMF (3 mL). The suspension was stirred vigorously at 60 °C. The reaction mixture was shielded from light with aluminum foil. After two days (reaction time unoptimized), the reaction mixture was cooled to room temperature, diluted with methanol, and filtered. The filtrate was evaporated to dryness and the crude product was purified by flash column chromatography (0% to 10% $MeOH/CH_2Cl_2$) to give **HoeNHBoc** as a light yellow solid (42 mg, 0.072 mmol, 61% yield). ^1H NMR (500 MHz, CD_3OD) δ 8.21 (s, 1H), 8.00 (d, J = 8.6 Hz, 2H), 7.91 (dd, J = 8.5, 1.2 Hz, 1H), 7.65 (d, J = 8.4 Hz, 1H), 7.50 (d, J = 8.8 Hz, 1H), 7.13 (d, J

= 1.8 Hz, 1H), 7.03 (two doublets, *J* = 8.6, 9.6 Hz, 2H + 1H = 3H), 4.03 (t, *J* = 6.1 Hz, 2H), 3.29–3.26 (m, 4H), 3.24 (t, *J* = 6.8 Hz, 2H), 2.93-2.87 (br, 4H), 2.55 (s, 3H), 1.94 (quintet, *J* = 6.5 Hz, 2H), 1.43 (s, 9H); ^{13}C NMR (125 MHz, CD_3OD) δ 162.5, 158.6, 155.3, 153.8, 149.1, 129.5, 125.5, 122.9, 122.5, 116.4, 116.0, 102.6, 80.0, 66.8, 55.8, 51.1, 45.3, 38.4, 30.7, 28.8; HRMS (ESI): calcd for $C_{33}H_{40}N_7O_3$ ($[M + H]^+$): 582.3187, found: 582.3201.

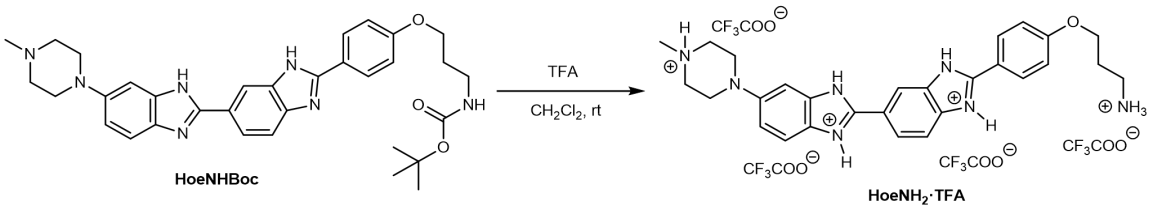

To a 10 mL round-bottom flask with **HoeNHBoc** (7.9 mg, 0.014 mmol) was added CH_2Cl_2 (0.5 mL) and TFA (0.5 mL). The suspension was stirred at room temperature for 1 h 10 min (reaction time unoptimized). Then toluene was added to the flask and the mixture was evaporated to dryness. **HoeNH$_2$·4TFA** salt was obtained as a brown oil and was used for the next step without further purification.

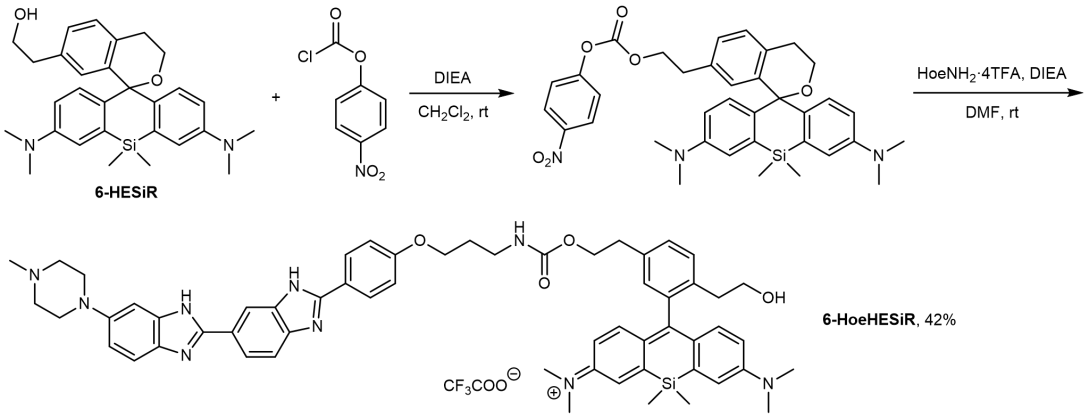

To a 10 mL round-bottom flask with **6-HESiR** (4 mg, 0.009 mmol) was added CH_2Cl_2 (0.4 mL) and DIEA (0.1 mL). 4-Nitrophenyl chloroformate (8.5 mg, 0.042 mmol) was added in one portion. The flask was sealed with a septum and stirred at room temperature overnight (reaction time unoptimized). On the next day, the reaction mixture was diluted with EA and quenched with water.

The mixture was stirred vigorously for 15 min and then washed with water and brine. The organic phase was dried over $MgSO_4$, filtered, and concentrated. This mixed carbonate crude product was transferred to a 10 mL round-bottom flask, which was kept under Ar. DMF (anhydrous, 0.5 mL) and DIEA (anhydrous, 0.2 mL) were added to this flask. The resulting solution was added to the 10 mL round-bottom flask with **HoeNH$_2$·4TFA** salt under Ar. The first flask with mixed carbonate was rinsed with DMF (anhydrous, 0.3 mL). The reaction mixture was stirred at room temperature overnight under Ar. On the next day, the reaction mixture was passed through a 0.2 µm syringe filter and diluted with water and acetonitrile (CH_3CN). The crude product was purified by preparative reverse phase HPLC (30% to 70% CH_3CN/H_2O with constant 0.1% TFA) to give **6-HoeHESiR** as a deep blue solid (4 mg, 0.004 mmol, 42% yield). ^{1}H NMR (500 MHz, CD_3OD) δ 8.37 (s, 1H), 8.07 (d, *J* = 8.5 Hz, 2H), 8.00 (d, *J* = 8.4 Hz, 1H), 7.85 (d, *J* = 8.5 Hz, 1H), 7.69 (d, *J* = 8.9 Hz, 1H), 7.42 (AB system, *J* = 8.9, 10.3 Hz, 2H), 7.37−7.27 (m, 4H), 7.12 (d, *J* = 9.8, 2H), 7.10 (d, *J* = 10.5 Hz, 2H), 7.03 (s, 1H), 6.76 (dd, *J* = 9.5, 1.7 Hz, 2H), 4.29 (t, *J* = 6.4 Hz, 2H), 4.06 (t, *J* = 5.8 Hz, 2H), 3.61-3.48 (br, 4H from the piperazine ring), 3.49 (t, *J* = 7.3 Hz, 2H), 3.42–3.29 (overlap with NMR solvent peak, 12H of the 4 methyl groups on 2 N atoms of the fluorophore structure), 3.28–3.24 (overlap with NMR solvent peak, 4H from the piperazine ring and 2H from a methylene group of the upper part of the fluorophore structure), 3.01 (s, 3H), 2.98 (t, *J* = 6.2 Hz, 2H), 2.52 (t, *J* = 7.3 Hz, 3H), 1.92 (quintet, *J* = 6.2 Hz, 2H), 0.60 (s, 3H), 0.57 (br, 3H); ^{13}C NMR (125 MHz, CD_3OD) δ 171.4, 164.0, 156.6, 151.0, 150.4, 143.7, 141.0, 138.8, 137.1, 132.1, 131.9, 131.6, 130.9, 129.9, 124.1, 122.9, 119.7, 117.2, 116.6, 115.9, 102.6, 67.8, 67.1, 63.8, 55.6, 44.4, 41.7, 39.6, 38.0, 36.9, 31.6, 31.5, 0.8, -0.7; HRMS (ESI): calcd for $C_{58}H_{66}N_9O_4Si$ (M^+): 980.5002, found: 980.5009.

^{1}H and ^{13}C NMR spectra of new compounds

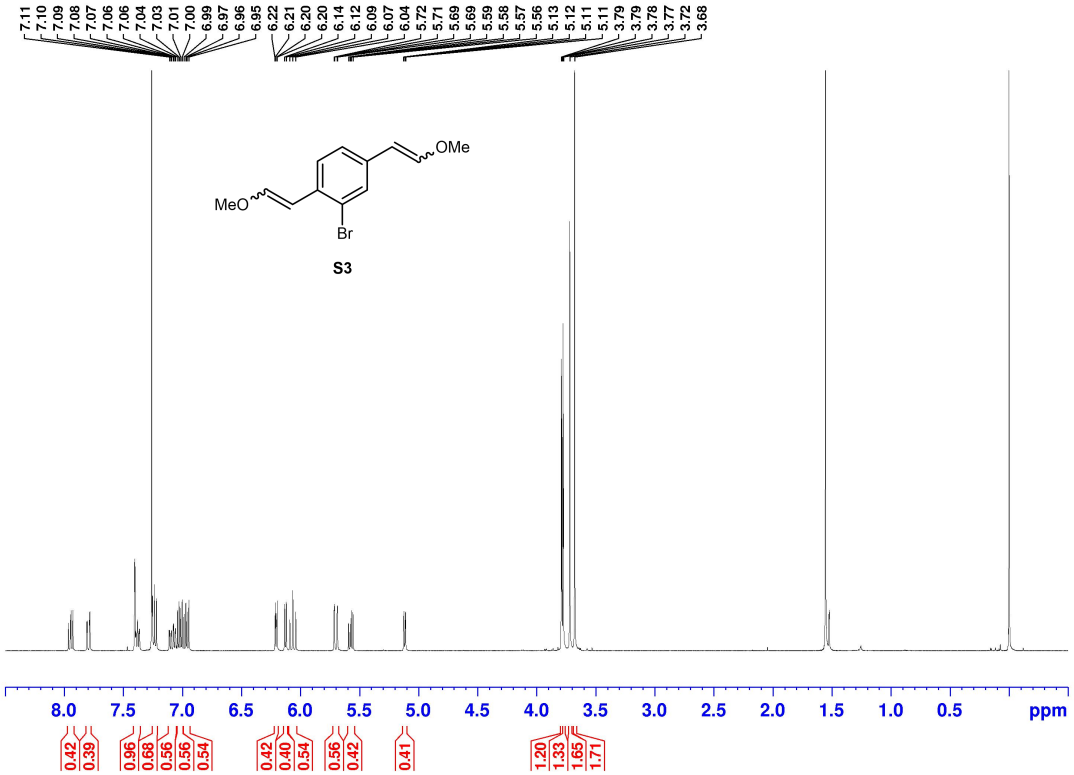

Current Data Parameters
NAME yzh-2-52H
EXPNO 1
PROCNO 1

F2 - Acquisition Parameters
Date_ 20180521
Time 15.39 h
INSTRUM spect
PROBHD Z119470_0274 (
PULPROG zg30
TD 32768
SOLVENT CDCl3
NS 16
DS 2
SWH 10000.000 Hz
FIDRES 0.610352 Hz
AQ 1.6384000 sec
RG 256
DW 50.000 usec
DE 6.50 usec
TE 296.5 K
D1 1.00000000 sec
TD0 1
SFO1 500.1330883 MHz
NUC1 1H
P1 8.03 usec
PLW1 14.00000000 W

F2 - Processing parameters
SI 65536
SF 500.1300117 MHz
WDW EM
SSB 0
LB 0.30 Hz
GB 0
PC 1.00

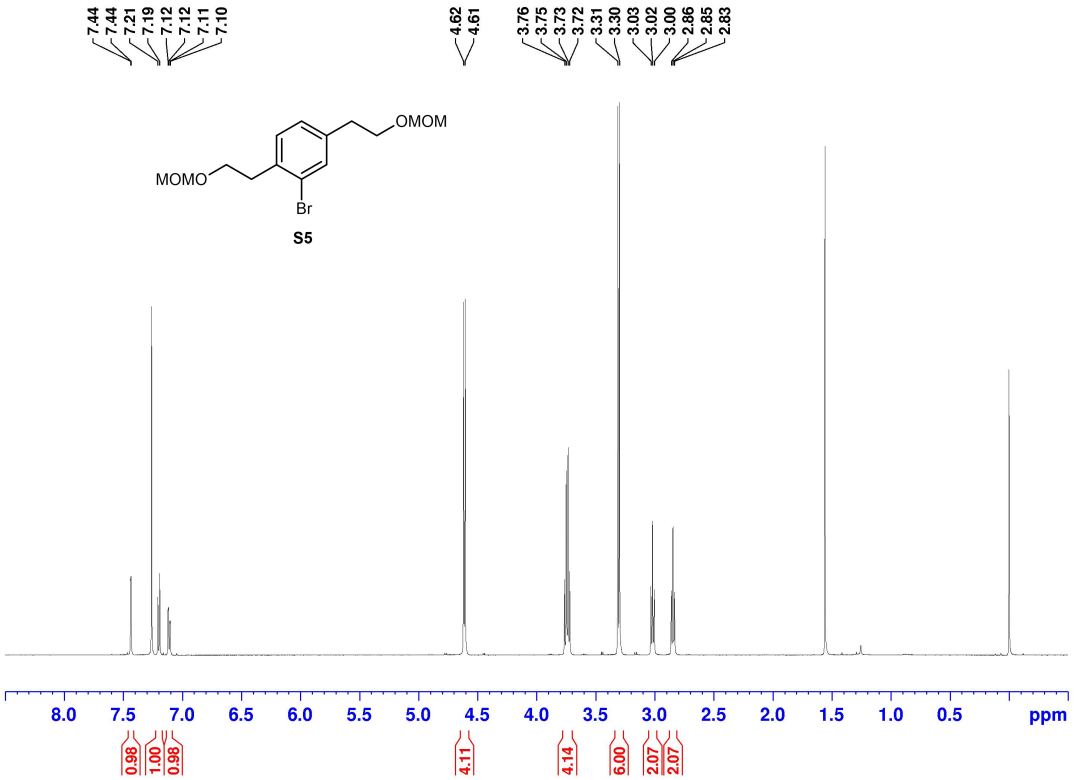

Current Data Parameters
NAME xrq-1-11H
EXPNO 1
PROCNO 1

F2 - Acquisition Parameters
Date_ 20200508
Time 13.47 h
INSTRUM spect
PROBHD Z119470_0274 (
PULPROG zg30
TD 32768
SOLVENT CDCl3
NS 27
DS 2
SWH 10000.000 Hz
FIDRES 0.610352 Hz
AQ 1.6384000 sec
RG 256
DW 50.000 usec
DE 6.50 usec
TE 298.0 K
D1 1.00000000 sec
TD0 1
SFO1 500.1330883 MHz
NUC1 1H
P1 8.03 usec
PLW1 14.00000000 W

F2 - Processing parameters
SI 65536
SF 500.1300120 MHz
WDW EM
SSB 0
LB 0.30 Hz
GB 0
PC 1.00

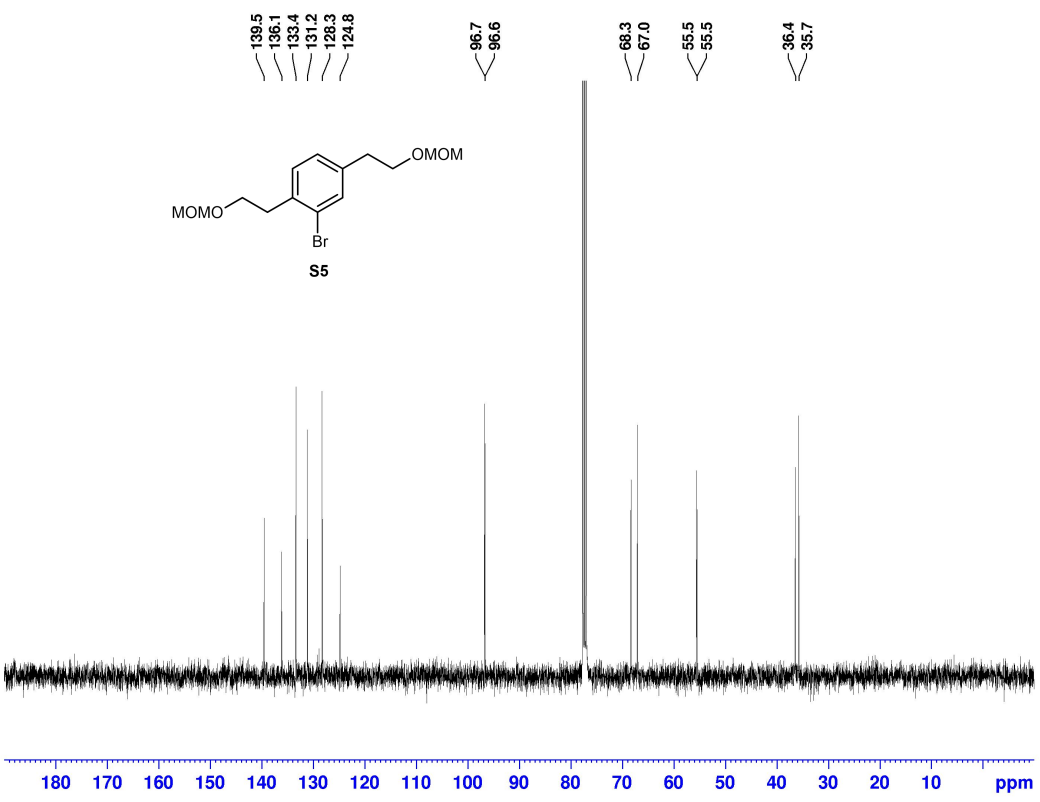

Current Data Parameters
NAME yzh-2-99C
EXPNO 1
PROCNO 1

F2 - Acquisition Parameters
Date_ 20180717
Time 10.27
INSTRUM spect
PROBHD 5 mm QNP 1H/1
PULPROG zgdc
TD 32768
SOLVENT CDCl3
NS 201
DS 0
SWH 25125.629 Hz
FIDRES 0.766773 Hz
AQ 0.6520832 sec
RG 26008
DW 19.900 usec
DE 20.00 usec
TE 0 K
D1 2.50000000 sec
d11 0.03000000 sec
MCREST 0 sec
MCWRK 0.01500000 sec

======== CHANNEL f1 ========
NUC1 13C
P1 9.50 usec
PL1 -5.00 dB
SFO1 100.6238364 MHz

======== CHANNEL f2 ========
CPDPRG[2 waltz16
NUC2 1H
PCPD2 80.00 usec
PL2 -4.00 dB
PL12 12.90 dB
SFO2 400.1320007 MHz

F2 - Processing parameters
SI 16384
SF 100.6127360 MHz
WDW EM
SSB 0
LB 1.00 Hz
GB 0
PC 1.40

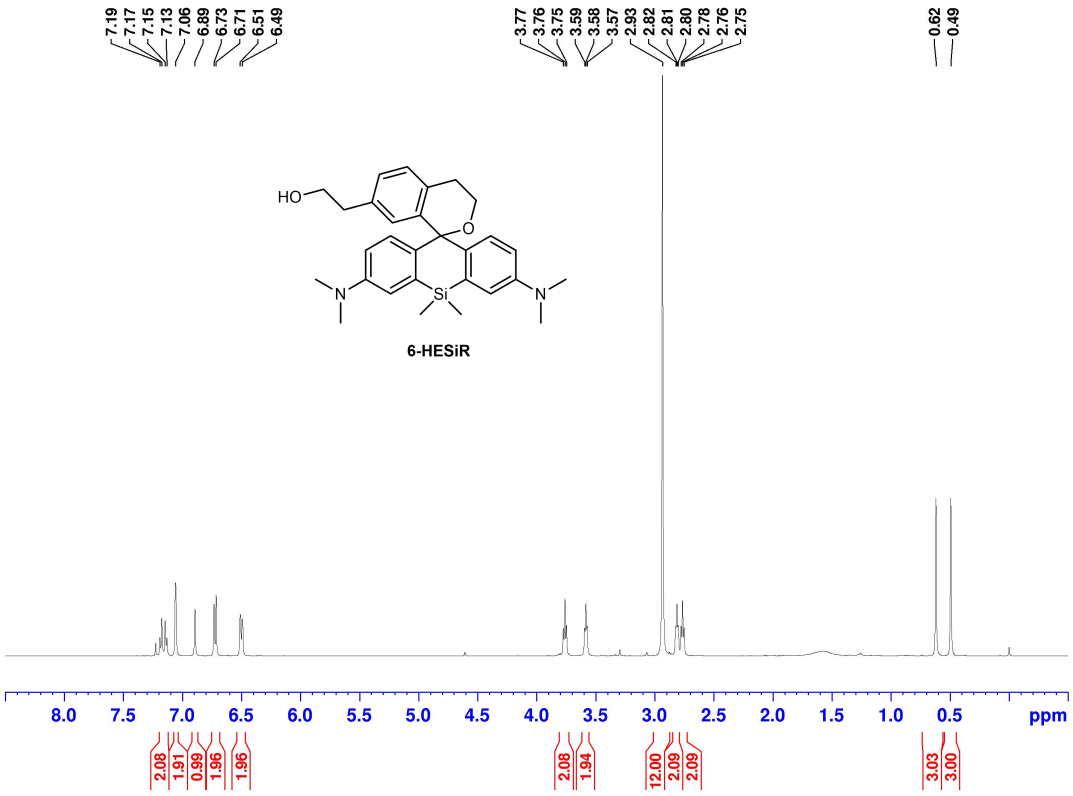

Current Data Parameters
NAME xrq-1-18H
EXPNO 5
PROCNO 1

F2 - Acquisition Parameters
Date_ 20200608
Time 13.43 h
INSTRUM spect
PROBHD Z119470_0274 (
PULPROG zg30
TD 32768
SOLVENT CDCl3
NS 32
DS 2
SWH 10000.000 Hz
FIDRES 0.610352 Hz
AQ 1.6384000 sec
RG 54.39
DW 50.000 usec
DE 6.50 usec
TE 295.4 K
D1 1.00000000 sec
TD0 1
SFO1 500.1330883 MHz
NUC1 1H
P1 8.03 usec
PLW1 14.00000000 W

F2 - Processing parameters
SI 65536
SF 500.1300291 MHz
WDW EM
SSB 0
LB 0.30 Hz
GB 0
PC 1.00

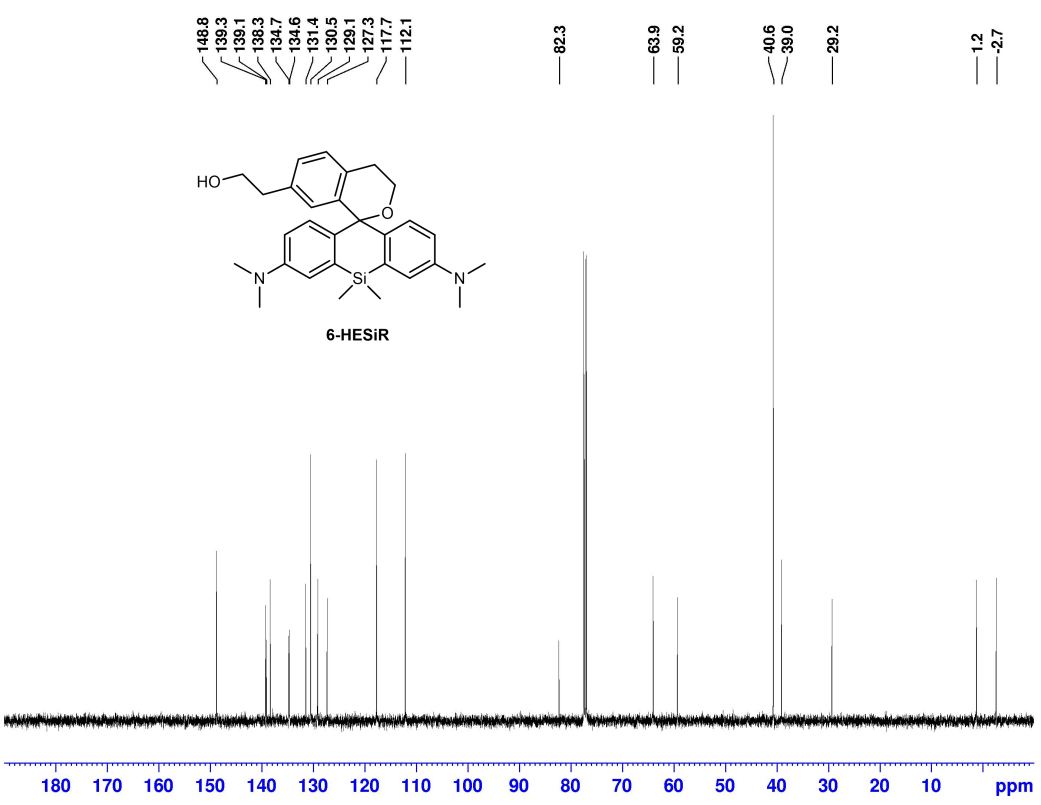

BRUKER

Current Data Parameters
NAME xrq-1-18C
EXPNO 1
PROCNO 1

F2 - Acquisition Parameters
Date_ 20200608
Time 14.26 h
INSTRUM spect
PROBHD Z119470_0274 (
PULPROG zgdc30
TD 32768
SOLVENT CDCl3
NS 30
DS 4
SWH 31250.000 Hz
FIDRES 1.907349 Hz
AQ 0.5242880 sec
RG 2050
DW 16.000 usec
DE 6.50 usec
TE 296.1 K
D1 2.00000000 sec
D11 0.03000000 sec
TD0 1
SFO1 125.7681547 MHz
NUC1 13C
P1 10.00 usec
PLW1 81.29100037 W
SFO2 500.1320005 MHz
NUC2 1H
CPDPRG[2 waltz16
PCPD2 80.00 usec
PLW2 23.04999924 W
PLW12 0.36015999 W

F2 - Processing parameters
SI 32768
SF 125.7577819 MHz
WDW EM
SSB 0
LB 1.00 Hz
GB 0
PC 1.40

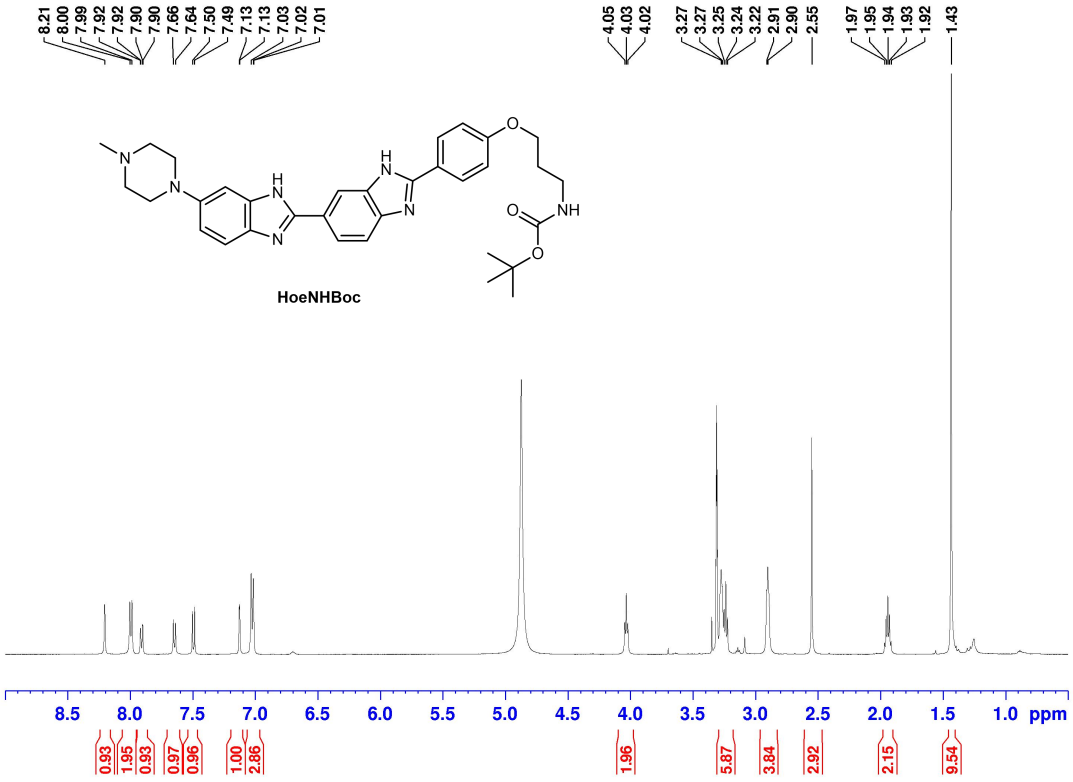

BRUKER

Current Data Parameters
NAME xrq-1-19H
EXPNO 2
PROCNO 1

F2 - Acquisition Parameters
Date_ 20200619
Time 14.11 h
INSTRUM spect
PROBHD Z119470_0274 (
PULPROG zg30
TD 32768
SOLVENT MeOD
NS 29
DS 2
SWH 10000.000 Hz
FIDRES 0.610352 Hz
AQ 1.6384000 sec
RG 117.5
DW 50.000 usec
DE 6.50 usec
TE 298.1 K
D1 1.00000000 sec
TD0 1
SFO1 500.1330883 MHz
NUC1 1H
P1 8.03 usec
PLW1 14.00000000 W

F2 - Processing parameters
SI 65536
SF 500.1300091 MHz
WDW EM
SSB 0
LB 0.30 Hz
GB 0
PC 1.00

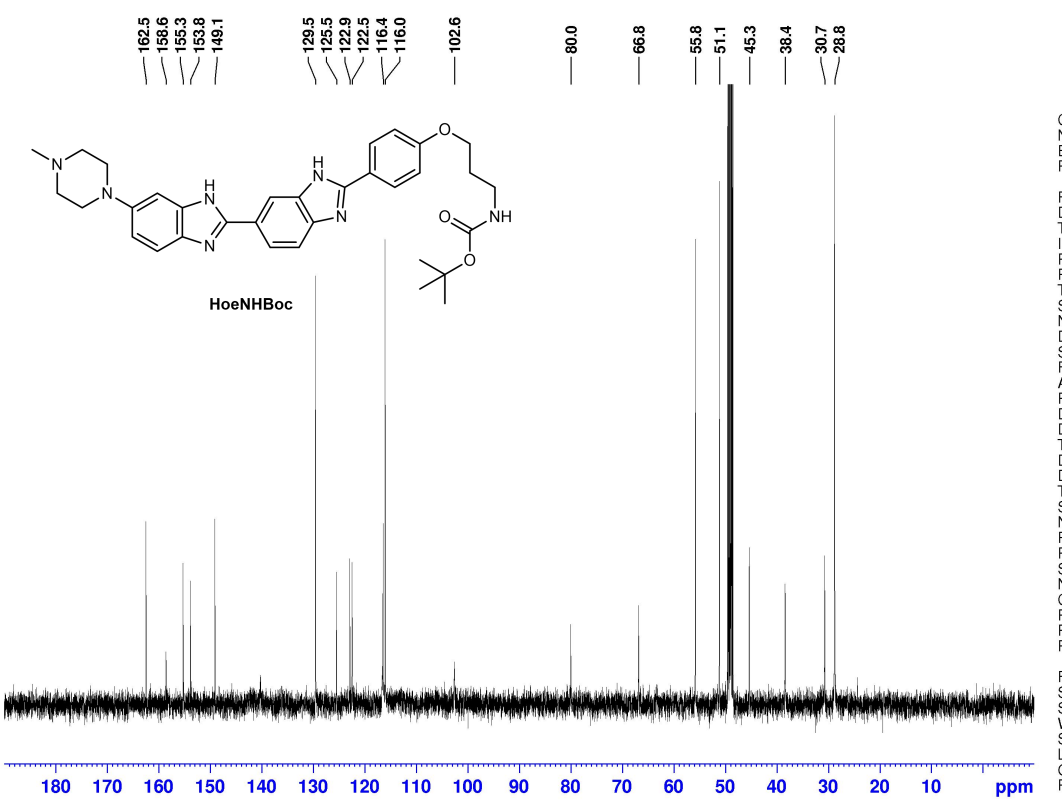

BRUKER

Current Data Parameters
NAME xrq-1-19C
EXPNO 5
PROCNO 1

F2 - Acquisition Parameters
Date_ 20200619
Time 16.45 h
INSTRUM spect
PROBHD Z119470_0274 (
PULPROG zgdc30
TD 32768
SOLVENT MeOD
NS 446
DS 4
SWH 31250.000 Hz
FIDRES 1.907349 Hz
AQ 0.5242880 sec
RG 2050
DW 16.000 usec
DE 6.50 usec
TE 298.7 K
D1 2.00000000 sec
D11 0.03000000 sec
TD0 1
SFO1 125.7681547 MHz
NUC1 13C
P1 15.00 usec
PLW1 96.75700378 W
SFO2 500.1320005 MHz
NUC2 1H
CPDPRG[2 waltz16
PCPD2 80.00 usec
PLW2 14.00000000 W
PLW12 0.14266540 W

F2 - Processing parameters
SI 32768
SF 125.7576144 MHz
WDW EM
SSB 0
LB 1.00 Hz
GB 0
PC 1.40

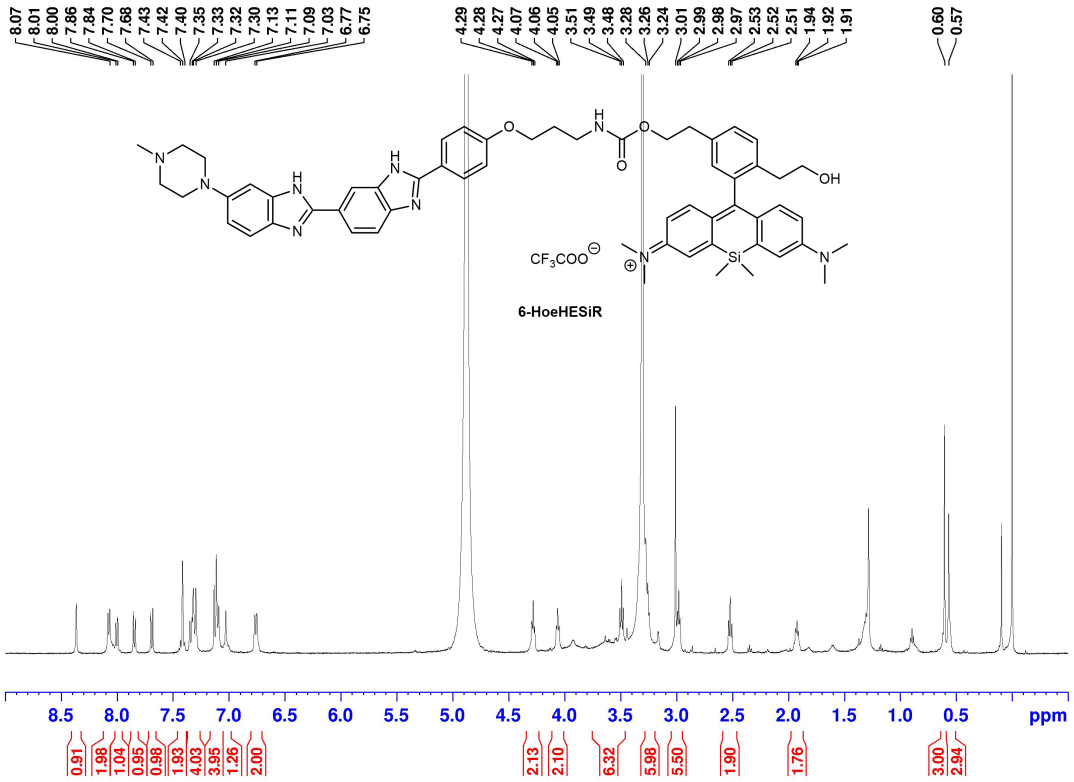

BRUKER

Current Data Parameters
NAME yzh-3-101H
EXPNO 3
PROCNO 1

F2 - Acquisition Parameters
Date_ 20191009
Time 10.44 h
INSTRUM spect
PROBHD Z119470_0274 (
PULPROG zg30
TD 32768
SOLVENT MeOD
NS 32
DS 2
SWH 10000.000 Hz
FIDRES 0.610352 Hz
AQ 1.6384000 sec
RG 131.75
DW 50.000 usec
DE 6.50 usec
TE 295.5 K
D1 1.00000000 sec
TD0 1
SFO1 500.1330883 MHz
NUC1 1H
P1 8.03 usec
PLW1 14.00000000 W

F2 - Processing parameters
SI 65536
SF 500.1300111 MHz
WDW EM
SSB 0
LB 0.30 Hz
GB 0
PC 1.00

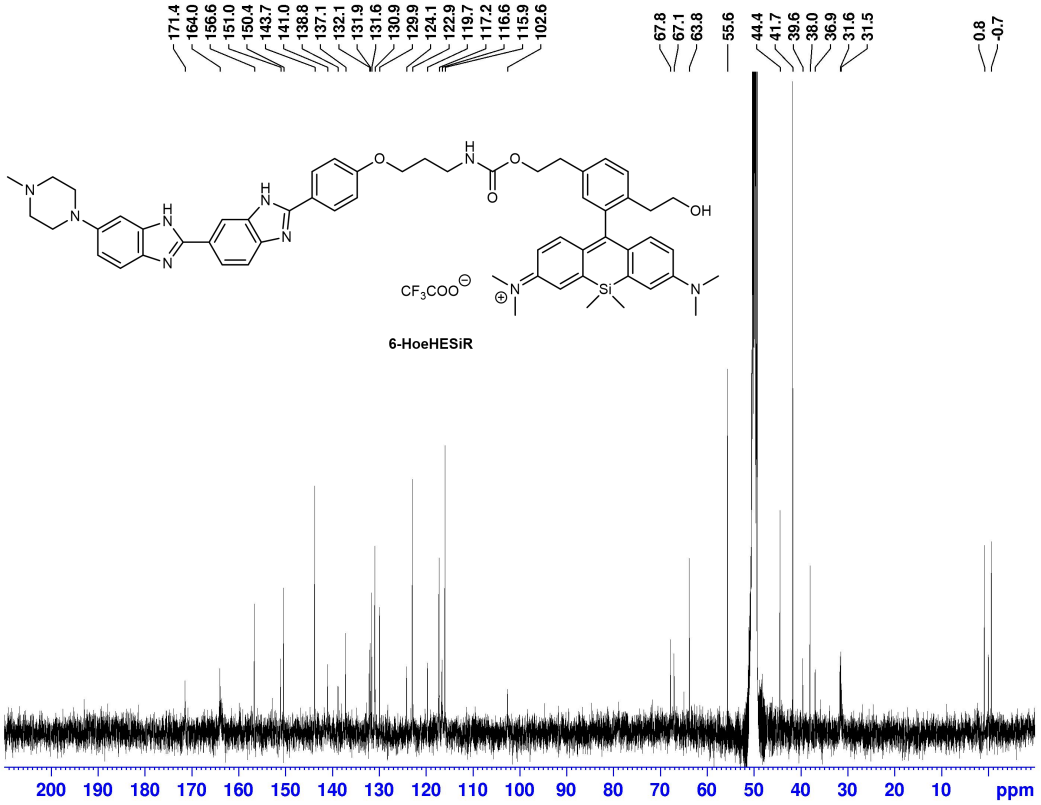

Current Data Parameters
NAME yzh-3-101
EXPNO 3
PROCNO 1

F2 - Acquisition Parameters
Date_ 20191009
Time 18.21
INSTRUM spect
PROBHD BBO 5mm Z3149/
PULPROG zgdc
TD 32768
SOLVENT MeOH
NS 15042
DS 1
SWH 31446.541 Hz
FIDRES 0.959672 Hz
AQ 0.5210112 sec
RG 9195.2
DW 15.900 usec
DE 6.00 usec
TE 0 K
D1 3.00000000 sec
d11 0.03000000 sec
MCREST 0 sec
MCWRK 0.01500000 sec

======== CHANNEL f1 ========
NUC1 13C
P1 11.00 usec
PL1 -2.00 dB
SFO1 125.7715724 MHz

======== CHANNEL f2 ========
CPDPRG[2 waltz16
NUC2 1H
PCPD2 100.00 usec
PL2 -6.00 dB
PL12 14.00 dB
SFO2 500.1312000 MHz

F2 - Processing parameters
SI 32768
SF 125.7575044 MHz
WDW EM
SSB 0
LB 1.20 Hz
GB 0
PC 1.00

Materials and methods

Photophysical properties of 6-HESiR and 6-HoeHESiR

Absorbance was measured on a Shanghai INESA L6S UV-Vis spectrophotometer. Fluorescence emission was measured on an Edinburgh Instruments FS5 Spectrofluorometer. The hpDNA (5'-CGCGAATTCGCGTTTTCGCGAATTCGCG-3') used for fluorescence titration of **6-HoeHESiR** was purchased from Sangon Biotech. It was prepared by denaturation and annealing in the Tris-HCl buffer (50 mM Tris-HCl, 100 mM NaCl, pH = 7.4) with a digital dry bath. The dsDNA samples used for fluorescence titration studies were prepared from corresponding complementary oligonucleotides (Sangon Biotech) by denaturation and annealing in the same Tris-HCl buffer with a digital dry bath. The fluorescence titration of probe binding sites was performed with 0.5 μM **6-HoeHESiR** in the same Tris-HCl saline buffer by sequential addition of the stock solutions of hpDNA and dsDNA.

Configuration of the microscope for 3D SMLM experiments

All 3D SMLM experiments were performed on a Nano BioImaging SRiS 2.0 STORM Super-resolution Microscope[5] (https://cpos.hku.hk/imaging-and-flow-cytometry-core/imaging-equipment; company: INVIEW , http://www.inview-tech.com). 3D imaging was performed with astigmatism according to the reported approach[6]. The detailed configuration is listed below.

- Lasers: 647 channel: 656 nm (500 mW); 750 channel: 750 nm (300 mW)
- Microscope base: Nikon eclipse Ti-E
- XY stage: manual manipulator stage, piezo stage insert
- Objective lens: CFI Aopchromat TIRF 100XH, N.A. 1.49, W.D. 0.12 mm, cover glass correction: 0.13-0.21 mm
- 3D lens (for astigmatism): f = 1000.0 mm, Ø1", N-BK7 Mounted Plano-Convex Round Cylindrical Lens (LJ1516RM, Thorlabs)
- Detector: Andor iXon Ultra 897 EMCCD Camera; two-channel simultaneous acquisition

with 320 × 160 pixels field of view

- Detection Band (647 channel, 656 nm laser): 672–712 nm (Model: FF01-692/40-25 made by Semrock)
- Dichoric mirror (for splitting between 647 and 750 channel): T760LPXR-UF2 (Chroma Technology Corp.)
- Software: Rohdea 2.0

Nucleosome and chromatin reconstitution

Recombinant histones H2A, H2B, H3, H4 and H1 were cloned and purified as previously described.[7] Reconstitution of histone octamers were performed as described previously.[8] Equimolar amounts of individual histones in unfolding buffer (7 M guanidinium HCl, 20 mM Tris-HCl, pH 7.5, 10 mM DTT) were dialyzed into refolding buffer (2 M NaCl, 10 mM Tris-HCl, pH 7.5, 1 mM EDTA, 5 mM 2-mercaptoethanol), and purified using Superdex S200 column. DNA templates of the 40–187bp DNA were cloned and purified as previously described.[8] Two single-stranded overhangs of DNA templates digested by BseYI enzyme were labeled with either dUTP-digoxigenin or dATP-biotin by Klenow reaction. Nucleosome samples were assembled using the salt-dialysis method as previously described.[8] Equimolar amounts of histone octamers and 40-187bp DNA templates were mixed in TEN buffers (10 mM Tris-HCl, pH 8.0, 1 mM EDTA, 2 M NaCl) and dialyzed for 17 hrs at 4 °C in TEN buffer, which was continuously diluted by slowly pumping in TE buffer (10 mM Tris-HCl, pH 8.0, 1mM EDTA) to lower concentration of NaCl from 2 M to 0.6 M. For histone H1 incorporation, histone H1 was added at this step and further dialyzed for 3 h. Samples were collected after final dialysis in HE buffer (10 mM HEPES, pH 8.0, 1 mM EDTA) for 4 h.

Electron microscopy analysis

Metal shadowing with tungsten for EM study was performed as described previously.[9] Reconstituted

nucleosome samples (2 ng/µl) were fixed with 0.4% glutaraldehyde in HE buffer on ice for 30 min. After 2 mM spermidine was added, samples were applied to glow-discharged carbon-coated EM grids and incubated for 2 min and then blotted. Grids were washed stepwise in 0%, 25%, 50%, 75%, and 100% ethanol solution for 4 min at room temperature, air dried and shadowed with tungsten at an angle of 10° with rotation. For the negative staining, the chromatin samples in fixative solution were incubated on glow-discharged carbon-coated EM grids for 1 min. The excess sample solution was removed using filter papers. The grid was incubated in 2% Uranylacetate for staining for 30 s twice, blotted with filter papers and allowed to air-dry for several minutes. The prepared EM samples were examined using a FEI Tecnai G2 Spirit 120 kV transmission electron microscope.

SMLM with spin-coated lambda DNA

Lambda DNA (Thermofisher, SD0011) was dissolved in 1 × TE50 buffer (pH = 7.5) to a concentration of 0.4 µg/mL and the solution was store at 4 °C. The stock solution of **6-HoeHESiR** was diluted in ddH_2O to the concentration of 0.1 µM and the solution was stored at 4 °C. A confocal dish (cellvis, D35-10-1-N) was incubated with 0.1 mg/mL poly-L-lysine (Sigma) for 1 h. Then the well in the dish was washed with ddH_2O three times and air-dried. The dish was fixed onto a spin-coater. The solution of lambda DNA (100 µL) was added to the dish. After 20 s of settling down, the spin speed was adjusted to 4000 rpm and kept for 60 s. During the spinning process, 2 mL ddH_2O was added. After spin-coating, the solution of **6-HoeHESiR** (100 µL) was added to the dish for imaging. SMLM experiment was carried out on a home-built microscope with an Olympus IX73 base, a 100× NA = 1.5 oil-immersion objective and an Andor iXon897 EMCCD camera. 10,000 frames were acquired with laser intensity of 3.5 kW/cm^2 at 671 nm, 50 ms camera exposure, and EM gain of 30.

3D SMLM of reconstituted nucleosomal arrays and 30-nm chromatin fibers

A sample of *in vitro* reconstructed 30-nm chromatin fibers (40 × 187 bp with H1 and biotin label) and a sample of *in vitro* reconstructed nucleosomal arrays (40 × 187 bp without H1) were prepared. Streptavidin (1 mg, Sigma Aldrich, S4762-1MG) was dissolved in 1 mL PBS (1 mg/mL). 5 µL of this stock solution was diluted in 400 µL MQ water. In a 35 mm culture dish (Corning), this diluted solution was loaded onto an 18 mm round coverslip (Marienfeld precision cover glass thickness No. 1.5H) which has been sequentially coated with 3 µm microbeads (Sigma Aldrich, 79166-5ML-F) and poly-D-lysine (Sigma Aldrich, P0899-50MG, MW = 70,000 – 150,000). After 10 min, the solution was removed, and the coverslip was washed with MQ water. The sample of reconstructed 30-nm chromatin fibers (2.5 µL, 63.1 ng/µL) was added to 400 µL HE buffer (10 mM HEPES, 1 mM EDTA, pH = 7.5) containing 2.5 µM **6-HoeHESiR**. The resulting solution was loaded onto the coverslip with immobilized streptavidin. After 10 min, the solution was replaced with 380 µL HE buffer. 3D SMLM of reconstituted 30-nm chromatin fibers was carried out in HE buffer at room temperature by applying 950 W/cm^2 excitation laser intensity at 656 nm. Exposure time of EMCCD camera was 17.7 ms/frame. 5,000 frames were acquired for each field of view. The sample of reconstituted nucleosomal arrays (1 µL, 69 ng/µL) was added to 400 µL HE buffer containing 2.5 µM **6-HoeHESiR**. The resulting solution was loaded onto the coverslip coated with poly-D-lysine. After 10 min, the solution was replaced with 380 µL HE buffer. 3D SMLM of reconstituted nucleosomal arrays was carried out in HE buffer at room temperature using the same set of imaging parameters. Real-time drift correction was applied by the active locking function of Rohdea software using the microbeads coated on coverslip.

Light-sheet microscopy of living HeLa cells

HeLa cells were cultured in DMEM (Dulbecco's Modified Eagle Medium, Gibco) supplemented with phenol red, 10% heat-inactivated fetal bovine serum (Gibco) and 1% penicillin/streptomycin (Gibco), at 37 °C with 5% CO_2. 5 mm coverslips (provided by Light Innovation Technology Ltd.)

were sonicated in 75% ethanol for 10 min, air-dried and placed in a 35 mm culture dish. Cells were typically seeded at a density of 0.5 or 1 × 10^5 cells/mL the day before imaging. On the day of imaging, Hela cells were incubated with **6-HoeHESiR** (5 μM for 30 min) and **6-HESiR** (2 μM for 30 min) in 1 mL DMEM at 37 °C with 5% CO_2. The cells were washed with DMEM once and placed back to the incubator with 1 mL DMEM in the dish. After 30 min, the cells were washed with DMEM once or twice before imaging. A coverslip with stained cells was placed in a sample holder and mounted. Live-cell 3D imaging was carried out in DMEM at 37 °C with 647-nm excitation laser and 30-ms camera exposure using a light-sheet microscope (Light Innovation Technology Ltd., LiTone LBS Light-sheet Microscope | litsite).

Cytotoxicity assay

HeLa cells were seeded in a 96-well plate at a density of 5000 cells/well and cultured in DMEM supplemented with phenol red, 10% heat-inactivated fetal bovine serum, 1% penicillin/streptomycin, and various concentrations of **6-HoeHESiR** at 37 °C with 5% CO_2. After 3 h, 10 μL of WST-1 reagent (Beyotime, C0036) was added to each well. After another 2 h, the absorbance readouts of each well were measured at 450 and 690 nm with a microplate reader (Thermo Varioskan LUX). Cell viability (%) data were obtained based on corrected absorbance values and a calibration curve of absorbance versus cell density.

3D SMLM of living HeLa cells

HeLa cells were cultured in DMEM supplemented with phenol red, 10% heat-inactivated fetal bovine serum and 1% penicillin/streptomycin, at 37 °C with 5% CO_2. A UV sterilized 18 mm round coverslip coated with 3 μm was placed in a 35-mm culture dish with coated face up. Cells were typically seeded at a density of 0.5 or 1 × 10^5 cells/mL the day before imaging. On the day of imaging, Hela cells were incubated with 5 μM **6-HoeHESiR** for 30 min in 1 mL DMEM at 37 °C

with 5% CO_2. The cells were washed with DMEM and placed back to the incubator with 1 mL DMEM in the dish. After 15–20 min, the cells were washed with DMEM before imaging. Live-cell 3D SMLM was carried out in 380 µL DMEM at room temperature by applying 3.2 kW/cm^2 or 950 W/cm^2 excitation laser intensity at 656 nm. Exposure time of EMCCD camera was 17.7 ms/frame. 5,000 frames were acquired for each field of view. Real-time drift correction was applied by the active locking function of Rohdea software using the microbeads coated on coverslip.

For treatments with HDAC inhibitors, HeLa cells were seeded on the day before imaging. Cells were treated with 200 nM TSA, 2 µM entinostat, and 1 µM ricolinostat for 20 h in DMEM, respectively. On the day of imaging, 3D SMLM experiments were carried out with the same experimental procedure and parameters as untreated cells.

3D SMLM of living chicken erythrocytes

20 µL chicken erythrocyte cell suspension (Innovative Research, 5% solution in Alsever's) was added to 1 mL DMEM containing 0.5 µM **6-HoeHESiR**. The suspended cells were incubated for 10 min in DMEM at 37 °C with 5% CO_2. The cells were centrifuged and DMEM was removed. Cells were washed with 1 mL HBSS (Hanks' Balanced Salt solution) and resuspended in 200 µL HBSS. The suspended cells in HBSS were loaded onto a microbead-coated coverslip having immobilized poly-D-lysine. The cells were allowed to settle down and attach to the coverslip for 5−10 min. Then the cell suspension was replaced with 380 µL HBSS. Live-cell 3D SMLM was carried out in HBSS at room temperature by applying 950 W/cm^2 excitation laser intensity at 656 nm. Exposure time of EMCCD camera was 17.7 ms/frame. 10,000 frames were acquired for each field of view. Real-time drift correction was applied by the active locking function of the Rohdea software using the microbeads coated on coverslip.

Chromatin image data analysis

Super-resolved images were generated by FIJI[10] with ThunderSTORM[11] plugin using "Normalized Gaussian" reconstruction algorithm. The result table of acquired localizations for each field of view was generated by the Rohdea software and directly used for chromatin image data analysis. Magnification ratio is set as 10.6 to give a 10-nm pixel size in reconstructed images. Original pixel size is 106 nm and original field of view is 320 pixel (width) × 160 pixel (height). Axial position is represented by RGB color depth coding. Axial range is set as –500 to 500 nm. XZ and YZ 3D projection images of representative chromatin fibers were generated by the chromatin fiber analysis program and by Volume Viewer plugin in FIJI (orange hot pseudo-color). Blinking and time-lapse videos were produced by FIJI. 3D rotation videos of representative chromatin fibers were produced by Volume Viewer plugin in FIJI (orange hot pseudo-color).

We have developed a computer program for quantitative analysis of chromatin fibers. The program performs automated analysis of molecular clusters as potential chromatin fibers based on a set of user-defined parameters. The source code of the computer program is available at https://github.com/HKU-BAL/Chromatin-Fiber-Imaging. The flowchart of the analysis is presented in Supplementary Fig. 12. The program takes in an input table that contains "the coordinates of localized single molecules", "localization precision", "photon count", and "frame number". First, the input data is processed by a preprocessing module, which is applied for: 1) filtering out the imprecise localizations with the precision threshold set as 30 nm; 2) magnifying the X and Y coordinates with the ratio of 10.6; 3) grouping the single molecules based on Z-coordinates into 10 nm per slice; and 4) split the data table into 250 or 500 frames a group for ease of analysis. Second, the XY projection image of one frame interval data table is rendered by the "average shifted histogram" algorithm with lateral shift set as 2 and axis shift set as 4. The localized single molecules are assigned to respective clusters according to their 8-way pixel connectivity in the X and Y-axes. A noise removal module that applies the "gray value thresholding strategy" and "outlier Z slice removing by max z gap tolerance" is used. To preserve maximum information, for each instance, both the original cluster

and the cluster after noise removal are kept for subsequent analyses. In the end, the XY, YZ, and XZ projection images of the identified clusters are rendered. For the identification of chromatin fibers with sufficient resolution and labeling density, we set up the following criteria: 1) continuous fibrous structure in YZ and XZ projection images; 2) number of localizations ≥ 10, resulting in labeling density ≥ 18,000 molecules/μm^3; 3) localization precision threshold of 15 nm; 4) maximum frame gap ≤ 40 frames; 5) maximum Z gap ≤ 50 nm. Long fiber diameter was the larger lateral FWHM value for each identified fiber. Short fiber diameter was the smaller lateral FWHM value for each identified fiber. Labeling density was calculated by the number of localizations for a chromatin fiber divided by its volume. The volume of a fiber is calculated by the total number of pixel cubes times the volume of each pixel cube, which is 10^{-6} μm^3. The resting/dwelling lifetime of a chromatin fiber was calculated by camera exposure 17.7 ms times the number of frames in which the localizations for that fiber were acquired.

The lateral and axial dimensions of a molecular cluster (a potential chromatin fiber) are estimated based on full width at half maximum (FWHM). To avoid potential bias in calculating FWHM, we adopted a "moving line" strategy. Using the estimation of the X dimension as an example, the process is illustrated in Supplementary Fig. 13a. The line moves on the cluster at the positions that cover the pixels at both the left and the right ends. The line width is set from 1 to the maximum that covers the whole cluster. Additionally, lines with too large FWHM fitting errors are discarded. The threshold is set as 6 for lateral FWHM and 30 for axial FWHM. The gray value submatrix within the line can be formulated as:

$$G_r = \begin{pmatrix} g_{i,j} & \cdots & g_{i,j+L} \\ \vdots & \ddots & \vdots \\ g_{i+w,j} & \cdots & g_{i+w,j+L} \end{pmatrix} \quad (1)$$

where w denotes the line width. L denotes the number of pixels horizontally of the cluster. i, j represents the upper left position of the cluster. $g_{i,j}$ denotes the gray value at the position (i,j)

Then, the data points (**X**, **Y**) can be presented as:

$$\mathbf{X} = (x_0, x_1, ..., x_L) \quad (2)$$

$$x_k = (k - i) * a \quad (3)$$

$$\mathbf{Y} = (y_0, y_1, ...y_L) \quad (4)$$

$$y_k = \frac{\sum_{v=0}^{w} g_{i+v,k}}{w} \quad (5)$$

where x_k denotes the distance between the k^{th} position and the most left position of the line. a represents the size of one pixel in the nanometer scale, which is 10 in this study. y_k denotes the normalized gray value at x_k.

The FWHM of a molecular cluster is estimated by fitting a Gaussian curve:

$$y = y_0 + Ae^{-\frac{(x-x_c)^2}{2\omega^2}} \quad (6)$$

The parameters are initiated by:

$$y_0 = min\,(\mathbf{Y}) \quad (7)$$

$$A = max(\mathbf{Y}) - min\,(\mathbf{Y}) \quad (8)$$

$$x_c = \mathbf{X}_{argmax\,(\mathbf{Y})} \quad (9)$$

$$\omega = std(\mathbf{X}) \quad (10)$$

Then, the curve fitting is optimized by the Levenberg-Marquardt algorithm.

Finally:

$$FWHM = 2\sqrt{2ln2}\omega \quad (11)$$

$$FWHM_{err} = 2\sqrt{2ln2}\omega_{err}$$

The FWHM values are presented in two ways: 1) mean FWHM of all the lines, and 2) the FWHM with maximum line width.

To reduce potential "noise" signals close to the molecular clusters that might interfere with subsequent analysis, a "noise" removal module is utilized. The module consists of a "gray value thresholding" strategy and an "the outlier Z slice removing by max z gap tolerance" strategy (Supplementary information, Fig. 13b). The gray value thresholding is applied to XY, YZ and XZ

projections of an identified molecule cluster. The key principle is "divide and conquer". By removing the low gray value pixels, a large, connected cluster can be split into several smaller connected components and these components are analyzed by following the same process as the original cluster. On the other hand, the basic idea of the outlier Z slice removing strategy is to detect and discard the top and/or bottom localizations which are separated from nearest neighboring localizations by Z gaps.

Quantification and statistical analysis

Quantification and statistical analysis were performed with Microsoft Excel and Graphpad Prism 8. Statistical graphs were generated with Graphpad Prism 8.

References

1. Ohtake, Y. *et al.* Discovery of Tofogliflozin, a Novel C-Arylglucoside with an O-Spiroketal Ring System, as a Highly Selective Sodium Glucose Cotransporter 2 (SGLT2) Inhibitor for the Treatment of Type 2 Diabetes. *J. Med. Chem.* **55**, 7828-7840 (2012).
2. Xie, Z., Yoon, S.-J. & Park, S. Y. Synthesis of Highly Fluorescent and Soluble 1,2,4-Linking Hyperbranched Poly(arylenevinylene) Featuring Intramolecular Energy Funneling. *Adv. Funct. Mater.* **20**, 1638-1644 (2010).
3. Butkevich, A. N., Lukinavičius, G., D'Este, E. & Hell, S. W. Cell-Permeant Large Stokes Shift Dyes for Transfection-Free Multicolor Nanoscopy. *J. Am. Chem. Soc.* **139**, 12378-12381 (2017).
4. Fang, L. *et al.* Chemoproteomic Method for Profiling Inhibitor-Bound Kinase Complexes. *J. Am. Chem. Soc.* **141**, 11912-11922 (2019).
5. Huang, B., Wang, W., Bates, M. & Zhuang, X. Three-Dimensional Super-Resolution Imaging by Stochastic Optical Reconstruction Microscopy. *Science* **319**, 810-813 (2008).
6. Luger, K., Mäder, A. W., Richmond, R. K., Sargent, D. F. & Richmond, T. J. Crystal structure of the nucleosome core particle at 2.8 Å resolution. *Nature* **389**, 251-260 (1997).
7. Chen, P. *et al.* H3.3 actively marks enhancers and primes gene transcription via opening higher-ordered chromatin. *Genes Dev.* **27**, 2109-2124 (2013).
8. Li, W. *et al.* FACT Remodels the Tetranucleosomal Unit of Chromatin Fibers for Gene Transcription. *Mol. Cell* **64**, 120-133 (2016).
9. Zhao, T. *et al.* A user-friendly two-color super-resolution localization microscope. *Opt. Express* **23**, 1879-1887 (2015).
10. Schindelin, J. *et al.* Fiji: an open-source platform for biological-image analysis. *Nat. Methods* **9**, 676-682 (2012).

11. Ovesný, M., Křížek, P., Borkovec, J., Švindrych, Z. & Hagen, G. M. ThunderSTORM: a comprehensive ImageJ plug-in for PALM and STORM data analysis and super-resolution imaging. *Bioinformatics* **30**, 2389-2390 (2014).